-Research Article-

Unveiling reversibility and plasticity in cardiac hypertrophy: insights from a transverse aortic constriction-release model

Manabu Shiraishi MD, PhD[1*]

[1]Department of Cardiovascular Surgery, Saitama Medical Center, Jichi Medical University, Saitama, Japan

***Corresponding Author:**

E-mail: manabu@omiya.jichi.ac.jp

Abstract

Transverse aortic constriction (TAC) is a well-established animal model used to study the pathomechanisms of pressure overload-induced heart failure. A number of studies have shown that treatment of the heart failure in this model may reverse the associated hypertrophy and fibrosis. However, because no TAC-release model in which hemodynamics improve upon alleviation of the physical stenosis has yet been established, the histologic changes and regulatory molecular biological mechanisms underlying the reversibility of cardiac hypertrophy and fibrosis are unknown. This study was conducted to establish an animal TAC-release model and thereby investigate the mechanisms that govern reversibility and plasticity of myocardial hypertrophy, fibrosis, and angiogenesis. TAC surgery was performed on rats, and 4 weeks later TAC release was achieved by cutting the constricting threads. TAC-subjected heart exhibited severe myocardial hypertrophy, fibrosis, and increased angiogenesis, along with diastolic dysfunction. Heart released from TAC showed reduced hypertrophy and fibrosis and improved diastolic function. Gene expression analysis uncovered regulator of calcineurin 1 (*Rcan1*) as a key player in cardiac function and histologic changes after TAC release. *Rcan1* knockdown exacerbated myocardial hypertrophy and fibrosis in heart released from TAC. The left ventricular afterload relief model revealed that increased oxidative stress and *Rcan1*

upregulation, which suppresses the calcineurin-NFAT pathway, are key to structural and functional recovery from pressure overload-induced cardiac hypertrophy.

Keywords

Heart failure, Hypertrophy, Fibrosis, Angiogenesis, Transverse aortic constriction, Reversibility

42 **Introduction**

43 Left ventricular pressure overload, as represented by systemic hypertension and aortic stenosis,
44 induces progressive fibrosis, markedly decreasing myocardial compliance, often leading to
45 lethal outcomes[1]. Animal models, such as transverse aortic constriction (TAC), have been
46 developed to study the pathophysiology of pressure overload-induced heart failure, with
47 numerous experiments exploring the underlying cellular and molecular mechanisms[2-4] . Elevated
48 pressure in the left ventricle triggers the binding of stress hormones, especially angiotensin II
49 and noradrenaline, to myocardial cell surface receptors, activating intracellular signaling
50 pathways. This culminates in increased expression of transcription and cell growth factors,
51 inducing myocardial hypertrophy. However, interventions can block these pathways, inhibiting
52 cardiomyocyte apoptosis and impeding progression of the hypertrophy, thereby regulating
53 cardiac reversibility and plasticity[5, 6]. Myocardial fibrosis resulting from left ventricular pressure
54 overload impairs heart function by excessive accumulation of extracellular matrix (ECM)
55 produced by activated myocardial fibroblasts[7, 8]. Extensive fibrosis is generally irreversible, but
56 studies have suggested the potential for reversal with treatment addressing underlying diseases
57 in experimental models[9, 10]. Cardiac hypertrophy has also been linked to accelerated
58 angiogenesis[11], which occurs to support increased myocyte proliferation and metabolism.
59 Although the mechanisms of reversibility of angiogenesis have not been fully clarified, it

appears that reducing cardiac overload and hypertrophy through appropriate treatment reverses angiogenesis by apoptosis-induced elimination of vascular cells and by decreasing growth factors, reducing inflammation and angiogenic demand[12]. Understanding the mechanisms responsible for reversibility and plasticity of myocardial hypertrophy, fibrosis, and angiogenesis is crucial for the development of heart failure therapies. However, understanding of the regulatory mechanisms involved in reversal of cardiac hypertrophy, fibrosis, and angiogenesis following hemodynamic changes remains incomplete because there is no animal model in which left ventricular pressure load resulting from the physical stenosis introduced by TAC is decreased. To bridge this gap in our understanding, a TAC-release model was created, allowing for comprehensive profiling of the structure, function, and histology of the heart. The goal was to elucidate the molecular mechanisms underlying reversibility and plasticity particular to myocardial hypertrophy, fibrosis, and angiogenesis.

Results

Characteristics of heart released from TAC

To elucidate the mechanism by which myocardial homeostasis is maintained in myocardial environments with under different hemodynamic loads, rats were divided into groups for establishment of the following conditions: a normal heart (NH) condition (for control), a

78 pressure-overload heart condition, with hearts by subjected to TAC (TAC-subjected heart), and
79 an overload relief condition, with removal of the constricting threads 4 weeks after TAC surgery
80 (heart released from TAC), as previously described[13] (Fig. 1a). M-mode echocardiography
81 revealed a significant increase in left ventricular posterior wall thickness at diastole (LVPWd),
82 reduction in left ventricular dimension at diastole and at systole (LVDd and LVDs), and volume
83 of TAC-subjected heart compared to measures in normal heart. These alterations improved in
84 heart released from TAC, seemingly due to a reduction in left ventricular afterload. Left
85 ventricular ejection fraction (LVEF) and other indicators of left ventricular contractility did not
86 differ significantly between conditions, presumably due to compensatory left ventricular
87 hypertrophy (Fig. 1b). The causes of these echocardiographic changes were then investigated in
88 terms of histology. A significant increase in the cross-sectional area around the short-axis of
89 individual cardiomyocytes (viewed from the transverse section) was observed in TAC-subjected
90 heart compared to that area in normal heart, and in heart released from TAC, the area decreased
91 to the size observed in normal heart (Fig. 1c). The amount of collagen deposition was
92 significantly increased in the TAC-subjected heart versus that in normal heart, and this increase
93 was attenuated in heart released from TAC (Fig. 1d). Capillary density was increased in TAC-
94 subjected heart and decreased in heart released from TAC (Fig. 1e). The data suggest that
95 hypertrophy of individual cardiomyocytes and increased collagen deposition in the interstitium

96 enhance left ventricular wall thickness and that angiogenesis is augmented by the increased
97 oxygen demand of the hypertrophied myocardium. Furthermore, the reduction in left ventricular
98 afterload effected by TAC release suppressed cardiac hypertrophy, fibrosis, and angiogenesis.
99 Interestingly, reversible histologic changes were observed in response to the hemodynamic
100 changes.

101 Expression of genes associated with myocardial hypertrophy, fibrosis, and angiogenesis was
102 examined next. Representative genes associated with cardiac hypertrophy (*Igf1, Mybpc3, Tnni3,*
103 *Tnnt2, Tpm1, Actc1, Myl2,* and *Myl3*) were upregulated in TAC-subjected heart in comparison
104 to expression of the same genes in normal heart. Expression of these genes was reduced in heart
105 released from TAC (Fig. 2a). This trend in gene expression was similar for genes associated
106 with fibrosis and angiogenesis. Expression of representative genes associated with fibrosis
107 (*Col1a1, Col3a1, Mmp2, Mmp9, Tgfb1, Acta2, Timp1,* and *Fn1*) and angiogenesis (*Vegfa, Fgf1,*
108 *Fgf2, Fgf9, Pdgfb,* and *Angpt2*) was upregulated in TAC-subjected heart in comparison to
109 expression in normal heart, whereas expression of these genes was downregulated in heart
110 released from TAC (Fig. 2b, c). Expression of genes that encode inflammatory cytokines TNFα
111 and IL1b, which play a role in promoting transcription of myocardial matrix metalloproteinases
112 (MMPs) and releasing latent Tgfb1 bound to the ECM, was similarly upregulated in TAC-
113 subjected heart and downregulated in heart released from TAC (Fig. 2d). Furthermore,

114 microarray analysis revealed the molecular signature of TAC-subjected heart and heart released
115 from TAC against that of normal heart. Genes with a twofold or greater increase or decrease in
116 expression between conditions were entered into Metascape, a gene annotation and analysis
117 resource (https://metascape.org/gp/index.html#/main/step1) [14]. A representative subset of terms
118 from the entire cluster was selected and transformed into a network layout, which characterized
119 changes in gene expression associated with muscle hypertrophy in response to stress, muscle
120 development, extracellular matrix organization, and blood vessel development to reflect
121 histologic changes in TAC-subjected heart and heart released from TAC (Supplementary Fig. 1;
122 the full dataset is available in the Gene Expression Omnibus [GEO] repository (GSE270186).
123

124 **Effects of oxidative stress following reperfusion**

125 Histologic features and expression of genes associated with myocardial hypertrophy, fibrosis,
126 and angiogenesis were significantly altered in TAC-subjected heart relative to those in normal
127 heart. However, these changes were reversed in heart released from TAC, with histologic
128 features and gene expression approximating those in normal heart. Based on these results and
129 the echocardiography-determined features, heart released from TAC appeared similar in
130 phenotype to that of normal heart. Interestingly, principal component analysis revealed a
131 difference in gene expression trends between normal heart and heart released from TAC,

132 differences that were as far apart as the differences in gene expression trends between normal
133 heart and TAC-subjected heart (Fig. 3a). Metascape was searched for relevant Gene Ontology
134 (GO) biological process terms[14] to determine which biological processes are involved in the
135 changes from TAC-subjected heart to heart released from TAC, with a focus on "response to
136 oxidative stress (GO: 0006979)" in heart released from TAC (Fig. 3b). The resolution of left
137 ventricular afterload by TAC release appeared to improve myocardial diastolic dysfunction,
138 increase diastolic coronary blood flow, and increase oxygen supply to the tissues. Tissue
139 damage due to increased oxygen supply from a state of relative chronic hypoxia to re-
140 oxygenation (reperfusion injury) was considered the main cause of elevated oxidative stress
141 levels in heart released from TAC. Oxidative stress during such reperfusion injury is likely due
142 in part to overproduction of reactive oxygen species (ROS). Mitochondria are the major source
143 of ROS production. Mitochondrial ROS (mtROS) account for the majority of ROS produced in
144 the cell. mtROS causes damage to the mitochondria themselves and increases permeability of
145 the mitochondrial membrane. This causes a rapid influx of calcium and other molecules into and
146 out of the mitochondria, inducing mitochondrial dysfunction[15-17]. mtDNA copy number, a
147 measure of mitochondrial function, was therefore assessed and found to be reduced in heart
148 released from TAC more than in TAC-subjected heart, suggesting association between the
149 increase in oxidative stress following reperfusion injury and decreased mitochondrial function

150 (Fig. 3c). Heatmaps generated by a group of genes associated with the GO biological process

151 term “response to oxidative stress“ revealed markedly accelerated expression of regulator of

152 calcineurin 1 (*Rcan1*), especially in heart released from TAC (Fig. 3d), a finding confirmed by

153 quantitative reverse transcription-polymerase chain reaction (qRT-PCR) (Fig. 3e). RCAN1 is

154 primarily responsible for (i) maintenance of mitochondrial function[18], (ii) inhibition of

155 inflammation[19], (iii) inhibition of Rho kinase activity[20], and (iv) inhibition of calcineurin-NFAT

156 signaling[20]. In this context, enrichment analysis was performed to clarify the role of *Rcan1* in

157 the oxidative stress state associated with reperfusion (the TAC-release condition). Genes with a

158 twofold or greater increase in expression in heart released from TAC compared to expression in

159 TAC-subjected heart were entered into Enricher, a comprehensive resource for curated gene sets

160 as well as a search engine (https://maayanlab.cloud/Enrichr/)[21]. The GO biological process

161 terms related to (i)–(iv) noted above were identified (Table 1). Of these, negative regulation of

162 calcineurin-NFAT signaling cascade (GO:0070885) was found to be a biological process

163 closely (though not significantly) related to the change from the TAC condition to the TAC-

164 release condition. The calcineurin-NFAT signaling cascade is a stress response in which

165 calcineurin activates NFAT transcription factors, leading to the expression of genes responsible

166 for hypertrophy, fibrosis, and angiogenesis. Activation of calcineurin-NFAT signaling by

167 oxidative stress simultaneously induces its own negative regulator, RCAN1[19]. The data obtained

168 indicate that activation of the calcineurin-NFAT signaling cascade due to oxidative stress
169 induced by reperfusion following absence of afterload in heart released from TAC is inhibited
170 by RCAN1. In other words, findings suggest the existence of a cardiac-specific homeostatic
171 mechanism effecting hypertrophy, fibrosis, and angiogenesis, with RCAN1 as one of the key
172 regulators (Fig. 3f).
173
174 **RCA1 is a potential regulator of cardiac remodeling**
175 To affirm the importance of *Rcan1* in the regulatory mechanism of myocardial hypertrophy,
176 fibrosis, and angiogenesis in myocardial environments with different hemodynamic loads,
177 hearts released from TAC were transfected *in vivo* with negative control small interfering RNA
178 (NC siRNA) or *Rcan1* siRNA (Fig. 4a). Results were as follows: Expression of *Rcan1* was
179 confirmed to be decreased in *Rcan1* siRNA-transfected heart (Fig. 4b). M-mode
180 echocardiography performed 4 weeks after TAC surgery revealed a significant increase in left
181 ventricular wall thickness and a reduction in left ventricular volume and LVEF in TAC-
182 subjected heart compared to measures in normal heart. Subsequently, in NC siRNA-transfected
183 heart, echocardiography performed at 8 weeks showed improvement in these alterations.
184 However, an increase in left ventricular wall thickness and a reduction in left ventricular volume
185 and LVEF were seen in *Rcan1* siRNA-transfected heart, compared to measures in NC siRNA-

186 transfected heart (Fig. 4c, d). In *Rcan1* siRNA-transfected heart, the weight change ratio was
187 significantly reduced compared to that of normal heart and of NC siRNA-transfected heart (Fig.
188 5a), suggesting cardiac cachexia due to reduced cardiac function as a cause. Histology was then
189 investigated. Extracted heart weight corrected for body weight did not differ between normal
190 heart and NC siRNA-transfected heart but was significantly increased in *Rcan1* siRNA-
191 transfected heart (Fig. 5b). Interventricular septum thickness in NC siRNA-transfected heart
192 was similar to that in normal heart but significantly increased in the *Rcan1* siRNA-transfected
193 heart compared to that in both normal heart and NC siRNA-transfected heart (Fig. 5c). The
194 trend was the same as that of left ventricular wall thickness. The cross-sectional area around the
195 short-axis of individual cardiomyocytes (Fig. 5d), amount of collagen deposition (Fig. 5e), and
196 capillary density (Fig. 5f) were significantly increased in *Rcan1* siRNA-transfected heart.
197 Increased (though not always significantly increased) expression of hypertrophy-related genes
198 (*Igf1, Mybpc3, Tnni3, Tnnt2, Tpm1, Actc1,* and *Myl3*) (Fig. 6a), fibrosis-related genes (*Col1a1,*
199 *Col3a1, Mmp2, Tgfb1, Timp1,* and *Fn1*) (Fig. 6b), and angiogenesis-related genes (*Fgf1, Fgf2,*
200 and *Angpt2*) (Fig. 6c) in heart released from TAC transfected with *Rcan1* reflected an increased
201 cross-sectional area around the short-axis of individual cardiomyocytes, increased amount of
202 collagen deposition, and increased capillary density. Briefly, *Rcan1* knockdown attenuated
203 cardiac reversibility and plasticity in heart released from TAC. Thus, *Rcan1* appears to be a

204 principal gene regulating the reversibility and plasticity of cardiomyocyte hypertrophy, fibrosis,

205 and angiogenesis in heart released from TAC.

206

207 **Discussion**

208 Cardiac hypertrophy frequently causes structural and functional modifications in the heart,

209 including changes in coronary blood flow, which can lead to reduced flow due to diastolic

210 failure and impaired myocardial perfusion[22]. Resolution of the hypertrophy, whether via

211 therapeutic interventions or adaptive mechanisms, can lead to reperfusion of previously

212 ischemic or hypoxic myocardial tissue. Although reperfusion restores blood flow to these areas,

213 it can also induce oxidative stress and tissue damage through various mechanisms, such as ROS

214 overproduction and inflammation[23]. Inflammatory cells and mediators contribute to oxidative

215 stress through pathways including nicotinamide adenine dinucleotide phosphate oxidase

216 activation and ROS release[24]. Additionally, cardiac hypertrophy is linked to changes in

217 mitochondrial function[25]. Resolving hypertrophy may enhance mitochondrial function, but it

218 can temporarily disrupt mitochondrial homeostasis, leading to ROS production and oxidative

219 stress[26]. In myocardium, ROS are constantly produced by a variety of enzymes, including

220 mitochondrial electron transfer enzymes, and under physiological conditions ROS in myocardial

221 tissue are maintained at low levels by intrinsic antioxidant mechanisms. However, during

222 reperfusion injury, overproduction of ROS results in a state of oxidative stress[15]. The ROS
223 induce opening of the mitochondrial permeability transition pore, which leads to cell death by
224 activation of the apoptotic pathway, resulting in mitochondrial dysfunction, which in turn
225 produces mtROS[17]. Indeed, mtROS production during reperfusion injury correlates with
226 reduced myocardial function and myocyte death[16]. The study described herein revealed the
227 following as a possible mechanism inducing oxidative stress under TAC release: (1) reversal of
228 the physical stenosis created by TAC decreasing left ventricular afterload and increasing
229 coronary reperfusion; (2) increased oxidative stress through the production of ROS; and (3)
230 mitochondrial dysfunction resulting in the production of mtROS, further contributing to the
231 oxidative stress.

232 The calcineurin-NFAT (nuclear factor of activated T cells) signaling pathway that was
233 suggested by results of the enrichment analysis to relate to phenotypic change is integral to
234 various physiological processes, including immune response and oxidative stress. Calcineurin, a
235 calcium/calmodulin-dependent phosphatase, activates NFAT transcription factors, leading to the
236 expression of genes responsible for cardio-structural alterations. NFAT proteins are typically
237 located in the cytoplasm in a phosphorylated, inactive state. ROS can directly activate
238 calcineurin, prompting dephosphorylation and subsequent nuclear translocation of NFAT
239 proteins. Once dephosphorylated by calcineurin, NFAT proteins move from the cytoplasm to

240 the nucleus, where they act as transcription factors regulating genes involved in myocardial

241 hypertrophy[27]. Activation of the calcineurin-NFAT pathway by ROS or oxidative stress

242 contributes to pathological cardiac remodeling and heart failure.

243 Genes such as *Igf1* (insulin-like growth factor 1)[28], *Mybpc3* (myosin binding protein C)[29],

244 *Tnni3* (troponin I)[30], *Tnnt2* (troponin T)[31], *Tpm1* (tropomyosin 1)[31], *Actc1* (actin alpha cardiac

245 muscle 1)[32], *Myl3* (myosin light chain 3)[33], and *Myl2* (myosin light chain 2)[34] are crucial for

246 cardiac hypertrophy. In response to various stimuli, expression of these genes is upregulated,

247 causing cardiac hypertrophy and remodeling. In a comparison of normal heart, TAC-subjected

248 heart, and heart released from TAC, significant up-regulation of *Tnni3* was observed in TAC-

249 subjected heart and related to cardiac hypertrophy. Up-regulation, though not significant, of

250 *Igf1, Mybpc3, Tnnt2, Actc1, Myl2,* and *Myl3* was also observed. In comparison to both normal

251 heart and NC siRNA-transfected heart, *Rcan1* siRNA-transfected heart showed significantly

252 increased expression of *Mybpc3*, related to increased cardiac hypertrophy. Expression of *Igf1,*

253 *Tnnt2, Tpm1, Actc1,* and *Myl3* tended to be increased. The calcineurin-NFAT signaling pathway

254 is crucial for transcriptional regulation of *Igf1*[35] and *Mybpc3*[36]. However, transcriptional

255 regulation of other cardiac hypertrophy-related genes by the calcineurin-NFAT signaling

256 pathway was not clarified. The author speculates that *Rcan1* knockdown in heart released from

257 TAC affected the expression of other cardiac hypertrophy-related genes, including *Igf1* and

258 *Mybpc3*, whose transcriptional regulation mechanisms are already known, mainly by enhancing
259 the calcineurin-NFAT signaling pathway. To prove this, studies are needed to clarify the
260 association between transcriptional regulation of cardiac hypertrophy-related genes other than
261 *Igf1* and *Mybpc3* and the calcineurin-NFAT signaling pathway.

262 With the ECM being an essential component of myocardium, alterations in the ECM
263 significantly affect myocardial structure and function. The calcineurin-NFAT signaling pathway
264 regulates genes involved in cardiac fibrosis, including collagen genes such as *Col1a1* (collagen
265 type I alpha 1 chain), *Col3a1* (collagen type III alpha 1 chain), *Mmp2* (matrix metallopeptidase
266 2), and *Mmp9* (matrix metallopeptidase 9) [37, 38]. This pathway also influences *Tgfb1*
267 (transforming growth factor beta 1), *Acta2* (actin alpha 2, smooth muscle) [37]. Furthermore,
268 inflammatory cytokines such as TNFa (tumor necrosis factor alpha) and IL1b (interleukin-1
269 beta) drive the transcription of MMPs in the myocardium[39], releasing latent TGFB1 bound to
270 the ECM. Therefore, besides the calcineurin-NFAT signaling pathway, increased expression of
271 inflammatory cytokines in TAC-subjected heart and its decreased expression in heart released
272 from TAC may have affected the regulation of MMP and TGFB1 expression. TGFB1 then
273 activates the Smad signaling pathway in fibroblasts, promoting the production of fibrous
274 collagens type I and III, key components of the ECM[40-42]. ACTA2, a marker of activated
275 myofibroblasts, is crucial in cardiac fibrosis, enhancing myofibroblast differentiation and the

276 contractile and matrix-producing abilities of fibroblasts. FN1 (fibronectin 1), another significant
277 ECM protein, is upregulated in cardiac fibrosis. Because MMP2 and MMP9 are downstream
278 factors of ROS and inflammatory cytokines TNFa and IL-1b, their expression and activity
279 increase during myocardial remodeling, promoting interstitial fibrosis. Studies on MMP2-
280 deficient mice have shown reduced myocardial hypertrophy and fibrosis in response to
281 hypertension and cardiac pressure overload[43]. Similarly, MMP9 deficiency partially improves
282 myocardial hypertrophy and fibrosis after pressure overload[44], pointing to the pivotal roles of
283 MMP2 and MMP9 in fibrosis and ECM remodeling. MMPs are regulated by tissue
284 metalloproteinase inhibitors (TIMPs), and ECM remodeling is intricately related to the
285 MMP/TIMP balance[45]. Left ventricular fibrosis may result from both increased collagen
286 synthesis and reduced collagen degradation due to decreased collagenase activity, which is
287 associated with increased *Timp1* expression[46]. In TAC-subjected heart, increased collagen
288 synthesis and changes in *Timp1* and *Mmp* expression and the MMP/TIMP balance may have
289 promoted collagen deposition. Conversely, in heart released from TAC, changes in expression
290 of *Mmps* and *Timp1* and the balance between them may have suppressed left ventricular
291 fibrosis. MMPs and TIMPs may also individually influence fibroblast behavior and ECM
292 production. Therefore, other regulatory mechanisms governing diverse fiber production need to
293 be elucidated for us to understand myocardial fibrosis.

294 The calcineurin-NFAT signaling pathway governs expression of essential angiogenic factors,
295 including VEGFA (vascular endothelial growth factor A)[47], FGF1 (fibroblast growth factor 1)
296 [48], PDGFB (platelet-derived growth factor beta)[49], and ANGPT2 (angiopoietin 2)[50]. VEGFA is
297 a potent inducer of angiogenesis, the process by which new blood vessels form from existing
298 ones. In cardiac hypertrophy, increased *Vegfa* expression leads to increased levels of VEGFA,
299 stimulating growth of new blood vessels in the heart. Whereas such angiogenesis initially meets
300 the heightened oxygen and nutrient demands of hypertrophic cardiac tissue, prolonged
301 angiogenesis can contribute to adverse remodeling and heart failure[51]. Thus, regulation of
302 VEGFA by the calcineurin-NFAT pathway plays a crucial role in balancing beneficial and
303 detrimental angiogenesis occurring with cardiac hypertrophy. FGF1, FGF2, and FGF9 are key
304 angiogenic factors that bind to fibroblast growth factor receptors, activating intracellular
305 signaling cascades[52]. Such binding promotes blood vessel formation and endothelial cell
306 proliferation, ensuring adequate blood supply to the expanding myocardium. PDGFB is crucial
307 for pericyte recruitment and vascular stabilization during angiogenesis. Secreted by endothelial
308 cells and other myocardial cells, PDGFB binds to receptors on pericytes and vascular smooth
309 muscle cells, promoting their recruitment to newly formed blood vessels[53]. ANGPT2 is a
310 context-dependent angiogenic factor that modulates vessel remodeling and maturation. Acting
311 as a competitive antagonist to ANGPT1, ANGPT2 disrupts the TIE2 receptor signaling pathway

312 and destabilizes endothelial cell junctions. This destabilization promotes vessel sprouting and
313 remodeling, facilitating angiogenesis in the myocardium[54]. Collectively, VEGFA, FGF,
314 PDGFB, and ANGPT2 play critical roles in regulating angiogenesis, ensuring proper vascular
315 adaptation with development of cardiac hypertrophy. The study reported herein revealed a
316 certain link between the transcriptional regulation of angiogenesis-related genes and the
317 calcineurin-NFAT signaling pathway in response to hemodynamic changes, but further studies
318 are needed.

319 *Rcan1* gene, known as regulator of calcineurin 1 gene, is a crucial inhibitor of the calcineurin-
320 NFAT signaling pathway, and it plays a role in preventing cardiac hypertrophy[20].
321 Overexpression of RCAN1 has been shown to attenuate pathological cardiac injury in
322 ischemia/reperfusion animal models by suppressing calcineurin-NFAT signaling and
323 hypertrophic gene expression. Conversely, decreased expression of RCAN1 is associated with
324 exacerbated cardiac injury[55]. Studies have shown that *Rcan1* expression is dynamically
325 regulated by oxidative stress during inflammation[19]. The present study on oxidative stress
326 through increased coronary blood flow with reduced left ventricular afterload and the regulation
327 of calcineurin-NFAT signaling activity by RCAN1 provided valuable insight into the molecular
328 mechanisms underlying cardiac reversibility and plasticity. RCAN1 can function as a pro-
329 survival factor, protecting cells from stress-induced apoptosis by inhibiting calcineurin-NFAT

330 signaling activation[18]. Thus, during increased oxidative stress associated with reperfusion,
331 RCAN1 may determine the balance between cell survival and cell death, not just effect cardiac
332 tissue remodeling. Optimal regulation of RCAN1 expression and activity is essential for
333 coordinating the cellular responses necessary for reversibility and plasticity mechanisms in
334 cardiac hypertrophy.

335 Understanding the role of ROS generation and oxidative stress due to reperfusion injury
336 following relief from left ventricular afterload has important therapeutic implications for cardiac
337 repair and regeneration strategies. Targeting oxidative stress or modulating RCAN1
338 expression/activity through gene therapy or pharmacological interventions could be potential
339 therapeutic approaches to attenuate cardiac hypertrophy and fibrosis and thereby improve
340 cardiac function. Further research in the form of preclinical and clinical studies is needed to
341 elucidate specific mechanisms and explore the therapeutic potential of targeting this axis.
342

343 **Limitations**

344 In the study described, markers of cardiac hypertrophy, fibrosis, and angiogenesis were assessed
345 by qRT-PCR, with total RNA from whole hearts used as starting material. Therefore, the results
346 do not allow for a conclusion whether the transcriptional differences originate from
347 cardiomyocytes, fibroblasts, or endothelial cells. Further studies are needed to isolate each cell

348 type from normal heart, TAC-subjected heart, and heart released from TAC and then run a cell-
349 by-cell analysis to determine the role of each cardiac component cell. Promotion of the
350 calcineurin-NFAT signaling pathway by suppression of RCAN1 expression was found to have a
351 significant effect on the cardiac tissue recovery process, i.e., suppression of RCAN1 expression
352 may exacerbate cardiac hypertrophy and fibrosis and promote angiogenesis. However, besides
353 regulating the calcineurin-NFAT signaling pathway, RCAN1 also regulates other pathways
354 involved in cardiac hypertrophy, fibrosis, and angiogenesis, including the RHO and TGFb
355 (transforming growth factor-beta) signaling pathways. Thus, it is uncertain whether
356 exacerbation of cardiac hypertrophy and fibrosis by *Rcan*1 knockdown in the TAC-release
357 model results solely from enhanced calcineurin-NFAT signaling.
358

359 **Conclusion**

360 A left ventricular afterload relief model was established by releasing TAC, and study of the
361 model shed light on the structural, functional, and histologic changes that occur in the heart
362 during the recovery from pressure overload-induced cardiac hypertrophy (Fig. 7). Increased
363 oxidative stress upon reperfusion and upregulation of the *Rcan1* gene, suppressing the
364 calcineurin-NFAT signaling pathway, are pivotal in the tissue repair process following heart
365 damage. Their intricate interaction dynamically influences cellular responses to injury,

366 inflammation resolution, and tissue remodeling. These study findings provide insight into
367 cardiac repair and regeneration. Further exploration in this realm may ultimately open novel
368 therapeutic avenues for managing heart disease.
369

370 **Materials and methods**

371 **TAC procedure and TAC release**

372 Animal experiments were conducted on approval of the Animal Experiment Committee in
373 accordance with the Animal Experiment Regulations of the Center for Experimental Medicine,
374 Jichi Medical University (Approval No. 21058-01). TAC surgery and TAC-release were
375 performed as previously reported but with some modifications[13, 56-58]. Animals used were male
376 Sprague Dawley rats (10 weeks old). Food and water were withheld 6 hours prior to surgery.
377 Surgical instruments were sterilized in an autoclave, and the surgical field was disinfected with
378 75% isopropyl alcohol. A heating pad was used during surgery, set to an appropriate
379 temperature (37°C) to maintain the animals' normal body temperature and thereby avoid rapid
380 changes in heart and respiratory rates. Inhalation anesthesia was achieved with a mixture of 2%
381 isoflurane and 100% oxygen at 0.5–1.0 L/min. Hairs on the animal's anterior neck and chest
382 were removed with depilatory cream. Each rat was positioned supine on the heating pad, with
383 their anterior teeth fixed over silk threads, the neck stretched, and limbs secured with paper

384 surgical tape. Anesthesia was maintained throughout the surgery by administration of 1.5–2%
385 isoflurane and 0.5–1.0 L/min 100% oxygen and confirmed by the toe-pinch test. The surgical
386 field was sterilized with 70% alcohol, and sterile drapes and gloves were used for each rat. Skin
387 incisions were made with a scalpel at the midline of the rat's neck and chest. The muscular layer
388 over the trachea was separated bilaterally. Partial sternotomy, up to the second rib, was
389 performed, and the sternum was separated with a chest retractor. The thymus was removed and
390 adipose tissue was gently detached from the aortic arch. After identification of the transverse
391 aorta, a 3-0 silk thread was passed between the brachiocephalic artery and left common carotid
392 artery with the use of sharp forceps. A loop of about 10 mm in diameter was created with 5-0
393 monofilament thread, and a 3-0 silk thread was passed through it (to indicate where to later cut
394 the silk thread for TAC-release). A 21-gauge blunt needle was placed parallel to the aorta, the 3-
395 0 silk thread was quickly tied to prevent loosening, and the needle was removed to produce
396 aortic stenosis. In control rats, procedures were the same, with the exception of aortic ligation.
397 The chest traction device was removed, the sternum was brought together with 4-0 silk thread,
398 and the skin was closed by continuous suturing with 6-0 monofilament. Postoperative analgesia
399 was provided by means of intraperitoneal buprenorphine injection. Anesthesia was gradually
400 lessened, and the rats were allowed to recover on a heating pad on signs of spontaneous
401 respiration. After full recovery, the rats were returned to their original housing room under a 12-

402 hour light/dark cycle and fed soft food. For pain relief, rats were given buprenorphine (0.1
403 mg/kg) intraperitoneally every 12 hours for 3 days. Four weeks after the transverse aortic
404 ligation, skin incisions were made at the neck and chest midline under inhalation anesthesia.
405 Adhesive scar tissue was dissected, and the silk thread ligating the aorta was identified by the
406 loop created with 5-0 monofilament thread. The 3-0 silk thread was cut, eliminating the
407 stenosis, taking care to avoid aorta damage. Procedures in the normal heart (NH), negative
408 control (NC), and TAC groups were performed similarly, with the addition of cutting the aortic
409 ligatures in the TAC-release (TAC-R) group. The chest was closed as in the initial surgery, and
410 postoperative pain was managed as described above.
411
412 **Echocardiography**
413 Cardiac function was assessed by means of transthoracic echocardiography at 4 and 8 weeks
414 after surgery. Echocardiography was performed with a Lumify L12-4 (Philips, Amsterdam,
415 Netherlands) Linear Array Ultrasound System equipped with a 12- to 4-MHz transducer. The
416 animals were anesthetized with isoflurane gas, and two-dimensional imaging of their hearts was
417 performed, with M-mode recordings acquired through the ventricular septum and posterior LV
418 wall. Interventricular septum and posterior wall thicknesses (both end-diastolic and end-
419 systolic) and LV internal dimensions were measured over at least three consecutive cardiac

420 cycles, according to established protocols[13, 59, 60]. LV volume was determined by M-mode

421 echocardiography; the left ventricular end-diastolic dimension (LVDd) and left ventricular end-

422 systolic dimension (LVDs) were measured on the parasternal short-axis view, assuming the left

423 ventricle to be a spheroid. LV volume was typically calculated according to the Teichholz

424 formula: $V = 7.0 \times D3 / (2.4 + D)$ [61]. Left ventricular stroke volume (LVSV) was derived by

425 subtracting left ventricular end-systolic volume (LVESV) from left ventricular end-diastolic

426 volume (LVEDV). LVEF was calculated as follows: $LVEF = SV \times 100 / LVEDV$ (%)[61]. Data

427 shown were derived from three independent measurements obtained in a blinded fashion.

428

429 **RNA extraction and RT-PCR**

430 Total RNA was extracted from rats' hearts with use of the Gene Jet PCR Purification Kit

431 (Thermo Fisher Scientific, Waltham, MA) and quantified with a Nano-Drop One

432 spectrophotometer (Thermo Scientific). For this RNA extraction, fresh tissue was excised from

433 the LV wall. cDNA was synthesized from 150 ng of total RNA extracted from heart tissues with

434 use of a High Capacity cDNA Reverse Transcription Kit (Applied Biosystems, Framingham,

435 MA). RT-PCR was performed with QuantStudio (Applied Biosystems) and SYBR Premix Ex

436 Taq II (Takara Bio, Shiga, Japan) reagent under the following conditions: 95°C for 30 seconds

437 followed by 40 cycles at 95°C for 5 seconds and 60°C for 30 seconds. Gene expression levels

438 were normalized to *Gapdh* (forward, 5'-CCCCTGGCCAAGGTCATCCA-3'; reverse, 5'-

439 CGGAAGGCCATGCCAGTGAG-3') expression. Gene expression data were acquired from

440 independent biological replicates. Primers were *Actc1* (forward, 5'-

441 TTTGGTGTGCGACAATGGCT-3'; reverse, 5'- TGCCCCATACCTACCATGAC-3'), *αSMA*

442 (forward, 5'-ACAACTGGTATTGTGCTGGACT-3'; reverse, 5'-

443 TGGCATGAGGCAGAGCATAG-3'), *Angpt2* (forward, 5'-AGTCAGGACTCACCACCAGT-

444 3'; reverse, 5'-CCTCCACCCATGTCCATGTC-3'), *Col1a1* (forward, 5'-

445 TGAGCCAGCAGATTGAGAAC-3'; reverse, 5'-CCAGTACTCTCCGCTCTTCC-3'), *Col3a1*

446 (forward, 5'-AGTCTGGAGTCGGAGGAATG-3'; reverse, 5'-

447 AGGATGTCCAGAGGAACCAG-3'), *Fgf1* (forward, 5'-CTTACCACAGCAGCAGGAATG-

448 3'; reverse, 5'- AACTGTCGATGGTGCGTTCA-3'), *Fgf2* (forward, 5'-

449 CTCTACTGCAAGAACGGCG-3'; reverse, 5'-ACTCCTCTCTCTTCTGCTTGGA-3'), *Fgf9*

450 (forward, 5'-GGAAAGACCACAGCCGATTC-3'; reverse, 5'-TGATCCATACAGCTCCCCCT-

451 3'), *Fn1* (forward, 5'-CGGAGGCCACCATCACTG-3'; reverse, 5'-

452 GTGGAAGGGTAACCAGTTGGG-3'), *Igf1* (forward, 5'-TACTTCAACAAGCCCACAGG-3';

453 reverse, 5'-CTCATCCACAATGCCTGTCT-3'), *Igfbp5* (forward, 5'-

454 AACGAAAAGAGCTACGGCGA-3'; reverse, 5'-GACCTTCGGGGAGTAGGTCT-3'), *Il1b*

455 (forward, 5'- TGGCAACTGTCCCTGAACTC-3'; reverse, 5'-

456 AAGGGCTTGGAAGCAATCCTTA-3'), *Mmp2* (forward, 5'-

457 AGAAGGCTGTGTTCTTCGCA-3'; reverse, 5'-AAAGGCAGCGTCTACTTGCT-3'), *Mmp9*

458 (forward, 5'-TGCCCTGGAACTCACACAAC-3'; reverse, 5'-GTTCACCCGGTTGTGGAAAC-

459 3'), *Mybpc3* (forward, 5'-AGGGCATGAAGCACGATGAA-3'; reverse, 5'-

460 AGCCAGTTCCACAGTAAGCC-3'), *Myl2* (forward, 5'-CAGCAGCCAGCCTCAGAC-3';

461 reverse, 5'-CCGTCTCTGTTCTGGTCCAT-3'), *Myl3* (forward, 5'-

462 AATCCTACCCAGGCAGAGGT-3'; reverse, 5'-TGTGCCCGTGTCTTTGTTCT-3'), *Pdgfb*

463 (forward, 5'-GGAGTCGGCATGAATCGCT-3'; reverse, 5'-ATGGAGTGGTCACTCAGCAT-

464 3'), *Rcan1* (forward, 5'-CTGCCCGTTGAAAAAGCAGAA-3'; reverse, 5'-

465 AATTTGGCCCTGGTCTCACTT-3'), *Tgfb1* (forward, 5'-CAACTTCTGTCTGGGACCCT-3';

466 reverse, 5'-CGGGTTGTGTTGGTTGTAGA-3'), *Timp1* (forward, 5'-

467 TTTCTGCAACTCGGACCTGG-3'; reverse, 5'-CGTCGAATCCTTTGAGCATCTTA-3'),

468 *TNFα* (forward, 5'- TCGTAGCAAACCACCAAGTG-3'; reverse, 5'-

469 TTGTCTTTGAGATCCATGCC-3'), *Tnni3* (forward, 5'-GGGACACCCTTCTAAGACCC-3';

470 reverse, 5'-CATCGCTGCTCTCATCCGC-3'), *Tnnt2* (forward, 5'-

471 CTGAGGCTGAGCAGACACC-3'; reverse, 5'-GCGTCAGACATGTTCTCCGT-3'), *Tmp1*

472 (forward, 5'-TCCAGCTGAAAGAGGCCAAG-3'; reverse, 5'-

473 CACATTTGCCTTCCGAGAGC-3'), and *Vegfa* (forward, 5'-GTACCTCCACCATGCCAAGT-

474 3'; reverse, 5'-GCATTCACATCTGCTGTGCT-3').

475

476 **mtDNA copy numbers**

477 Total DNA, including mtDNA, was extracted from heart tissue with use of the ISOSPIN Tissue

478 DNA Kit (NIPPON GENE, Tokyo, Japan) and quantified with a Nano-Drop One

479 spectrophotometer (Thermo Scientific). For DNA extraction from rat hearts, fresh tissue was

480 excised from the left ventricular wall. RT-PCR was performed with use of the QuantStudio

481 (Applied Biosystems) and SYBR Premix Ex Taq II (Takara Bio) under the following

482 conditions: 98°C for 2 minutes followed by 40 cycles at 98°C for 10 seconds, 60°C for 15

483 seconds, and 68°C for 30 seconds. RT-PCR was performed on one sample by using four primer

484 pairs, and the mtDNA copy number was calculated by relative quantification based on the

485 difference in cycle threshold values between mtDNA and nuclear DNA. Primers used were *mt-*

486 *ND1* (forward, 5'-ATCTGTGTTATTAGACATGCACCA-3'; reverse, 5'-

487 TAGTCACCCCCAGGACGAAT-3'), *mt-ND5* (forward, 5'-

488 ACATGCACCATTAAGTCATAAACCT-3'; reverse, 5'-ATAGTCACCCCCAGGACGAA-3'),

489 *SLCO2B1* (forward, 5'-TCAGCCCTTTGGCATCTCC-3'; reverse, 5'-

490 CATCATGGTCACTGCAAACAGG-3'), and *SERPINA1* (forward, 5'-

491 AGCCAGGGAGACAGGGA-3'; reverse, 5'-AGCCAGGGAGACAGGGA-3').

492

493 **Microarray analysis**

494 Total RNA was isolated from whole heart according to the aforementioned procedure and

495 analyzed by means of GeneChip technology (GeneChip Arrays platform with Clariom™ S

496 Assay, Rat; Thermo Fisher Scientific). Standard quality control steps were included to

497 determine total RNA quality with use of Agilent Bioanalyzer 2100 (RNA integrity number

498 (RIN) > 7.0; Agilent Technologies, Santa Clara, CA) and quantity with use of a nanoliter

499 spectrophotometer (Nanodrop, Thermo Fisher Scientific). Two independent biological

500 replicates were prepared from whole hearts. Median per-chip normalization was applied to each

501 array. Differentially expressed genes were identified at a fold-change cutoff of 2.0.

502

503 **Immunohistochemistry**

504 For immunohistochemical analysis, rats were euthanized by cervical dislocation, and this was

505 followed immediately by clamping of the aorta and injection of ice-cold PBS into the left

506 ventricular cavity. The heart was then perfused with ice-cold 4% paraformaldehyde in PBS.

507 Subsequently, the heart was excised, bisected at the midpoint along the short axis of the left

508 ventricle, embedded in optimal cutting temperature compound (VWR International, Radnor,
509 PA), and rapidly frozen in isopentane chilled in liquid nitrogen. Frozen tissue sections (8 μm
510 thick) were prepared, and non-specific antibody-binding sites were blocked with PBS
511 containing 5% goat serum. Antibodies were then applied overnight at 4°C: Griffonia
512 Simplicifolia I-Isolectin B4, DyLight 594 Conjugate at 1:100 dilution (DL-1207, Vector
513 Laboratories, Burlingame, CA) and anti-Cardiac Troponin T Ab at 1:00 dilution (15513-1-AP,
514 Proteintech, Rosemont, IL). Slides were washed and, if necessary, incubated with fluorophore-
515 conjugated secondary antibody at 1:300 dilution (Alexa Fluor 488-conjugated polyclonal
516 antibody, Invitrogen, Waltham, MA) and DAPI in blocking buffer for 1 hour at room
517 temperature. Data were acquired from independent biological replicates.
518
519 **Masson's Trichrome staining**
520 Frozen tissue sections (8 μm thick) were prepared as described above and stained with
521 trichrome (Trichrome Stain Kit, Scytek Laboratories, Logan, UT) according to the
522 manufacturer's instructions. Data were acquired from independent biological replicates.
523
524 **Imaging and analysis**

525 Digital images were captured with use of an all-in-one fluorescence microscope (BZ-8000;
526 KEYENCE, Osaka, Japan) and imported as TIFF files into ImageJ (National Institutes of
527 Health). Images were obtained from three separate regions, and the fibrin-positive area in each
528 region was quantified as a percentage of the total region area. The Color Threshold function in
529 ImageJ was used to measure the fibrin clot area. Initially, the image was divided into three parts
530 by means of the Split Channels function, and the clearest view of the target area was selected.
531 Subsequently, the threshold was adjusted and set to detect and highlight only the object of
532 interest (i.e., the fibrin clot area). The percentage of the object area in the image was then
533 calculated. This procedure was applied to both Control and target group images, with the
534 threshold value set for the Control group also used for the target group.
535
536 **In vivo transfection**
537 To investigate the role of RCAN1 in cardiac fibrosis, in vivo gene silencing was performed by
538 using *Rcan1* siRNA (AM16706, Invitrogen) along with a transfection reagent, according to a
539 previously described protocol[62] with modifications. Forty micrograms of siRNA, combined with
540 non-viral in vivo transfection reagent JetPEI® (Polyplus-transfection), was administered to each
541 animal three times per week by tail-vein injection. An N/P ratio of 8 in a total volume of 500 μL

542 of 5% dextrose was maintained for each injection, according to the manufacturer's protocol. NC

543 siRNA (AM4635, Invitrogen) was administered for negative control.

544

545 **Statistical analysis**

546 Statistical analysis was performed with GraphPad Prism version 8 (GraphPad Software, San

547 Diego, CA). Data were assumed to be normally distributed and are presented as mean ± SEM.

548 All statistical tests were parametric. For comparison between multiple sample sets, repeated-

549 measures analysis of variance (ANOVA) or one- or two-way ANOVA was performed, followed

550 by Bonferroni's post-hoc test. To evaluate differences between two sample sets, two-tailed,

551 unpaired Student's t-test was applied.

552

553 **References**

554 1. Writing Committee, M. et al. 2016 ACC/AHA/HFSA Focused Update on New
555 Pharmacological Therapy for Heart Failure: An Update of the 2013 ACCF/AHA
556 Guideline for the Management of Heart Failure: A Report of the American College of
557 Cardiology/American Heart Association Task Force on Clinical Practice Guidelines and
558 the Heart Failure Society of America. *Circulation* **134**, e282-293 (2016).
559 2. Rockman, H.A. et al. Segregation of atrial-specific and inducible expression of an atrial
560 natriuretic factor transgene in an in vivo murine model of cardiac hypertrophy. *Proc*
561 *Natl Acad Sci U S A* **88**, 8277-8281 (1991).
562 3. You, J. et al. Differential cardiac hypertrophy and signaling pathways in pressure versus
563 volume overload. *Am J Physiol Heart Circ Physiol* **314**, H552-H562 (2018).
564 4. Bao, D. et al. Tomoregulin-1 prevents cardiac hypertrophy after pressure overload in
565 mice by inhibiting TAK1-JNK pathways. *Dis Model Mech* **8**, 795-804 (2015).
566 5. Heineke, J. & Molkentin, J.D. Regulation of cardiac hypertrophy by intracellular
567 signalling pathways. *Nat Rev Mol Cell Biol* **7**, 589-600 (2006).
568 6. Hill, J.A. & Olson, E.N. Cardiac plasticity. *N Engl J Med* **358**, 1370-1380 (2008).
569 7. Janicki, J.S. & Brower, G.L. The role of myocardial fibrillar collagen in ventricular
570 remodeling and function. *J Card Fail* **8**, S319-325 (2002).
571 8. Kong, P., Christia, P. & Frangogiannis, N.G. The pathogenesis of cardiac fibrosis. *Cell*
572 *Mol Life Sci* **71**, 549-574 (2014).
573 9. Dewald, O. et al. Development of murine ischemic cardiomyopathy is associated with a
574 transient inflammatory reaction and depends on reactive oxygen species. *Proc Natl*
575 *Acad Sci U S A* **100**, 2700-2705 (2003).
576 10. Brilla, C.G., Matsubara, L. & Weber, K.T. Advanced hypertensive heart disease in
577 spontaneously hypertensive rats. Lisinopril-mediated regression of myocardial fibrosis.
578 *Hypertension* **28**, 269-275 (1996).
579 11. Broughton, K.M. et al. Mechanisms of Cardiac Repair and Regeneration. *Circ Res* **122**,
580 1151-1163 (2018).
581 12. Dimmeler, S. & Zeiher, A.M. Endothelial cell apoptosis in angiogenesis and vessel
582 regression. *Circ Res* **87**, 434-439 (2000).
583 13. Shiraishi, M., Suzuki, K. & Yamaguchi, A. Effect of mechanical tension on fibroblast
584 transcriptome profile and regulatory mechanisms of myocardial collagen turnover.
585 *FASEB J* **37**, e22841 (2023).
586 14. Zhou, Y. et al. Metascape provides a biologist-oriented resource for the analysis of
587 systems-level datasets. *Nat Commun* **10**, 1523 (2019).

588 15. Yellon, D.M. & Hausenloy, D.J. Myocardial reperfusion injury. *N Engl J Med* **357**,
589 1121-1135 (2007).
590 16. Chouchani, E.T. et al. A Unifying Mechanism for Mitochondrial Superoxide Production
591 during Ischemia-Reperfusion Injury. *Cell Metab* **23**, 254-263 (2016).
592 17. Hausenloy, D.J. & Yellon, D.M. Myocardial ischemia-reperfusion injury: a neglected
593 therapeutic target. *J Clin Invest* **123**, 92-100 (2013).
594 18. Duan, H. et al. Rcan1-1L overexpression induces mitochondrial autophagy and
595 improves cell survival in angiotensin II-exposed cardiomyocytes. *Exp Cell Res* **335**, 99-
596 106 (2015).
597 19. Norberg, K.J. et al. RCAN1 is a marker of oxidative stress, induced in acute
598 pancreatitis. *Pancreatology* **18**, 734-741 (2018).
599 20. Wang, S., Wang, Y., Qiu, K., Zhu, J. & Wu, Y. RCAN1 in cardiovascular diseases:
600 molecular mechanisms and a potential therapeutic target. *Mol Med* **26**, 118 (2020).
601 21. Chen, E.Y. et al. Enrichr: interactive and collaborative HTML5 gene list enrichment
602 analysis tool. *BMC Bioinformatics* **14**, 128 (2013).
603 22. Dellsperger, K.C. & Marcus, M.L. The effects of pressure-induced cardiac hypertrophy
604 on the functional capacity of the coronary circulation. *Am J Hypertens* **1**, 200-207
605 (1988).
606 23. Eltzschig, H.K. & Eckle, T. Ischemia and reperfusion--from mechanism to translation.
607 *Nat Med* **17**, 1391-1401 (2011).
608 24. Brandes, R.P., Weissmann, N. & Schroder, K. Redox-mediated signal transduction by
609 cardiovascular Nox NADPH oxidases. *J Mol Cell Cardiol* **73**, 70-79 (2014).
610 25. Tsutsui, H., Kinugawa, S. & Matsushima, S. Mitochondrial oxidative stress and
611 dysfunction in myocardial remodelling. *Cardiovasc Res* **81**, 449-456 (2009).
612 26. Murphy, E. & Steenbergen, C. Mechanisms underlying acute protection from cardiac
613 ischemia-reperfusion injury. *Physiol Rev* **88**, 581-609 (2008).
614 27. Molkentin, J.D. et al. A calcineurin-dependent transcriptional pathway for cardiac
615 hypertrophy. *Cell* **93**, 215-228 (1998).
616 28. Duerr, R.L. et al. Insulin-like growth factor-1 enhances ventricular hypertrophy and
617 function during the onset of experimental cardiac failure. *J Clin Invest* **95**, 619-627
618 (1995).
619 29. Page, S.P. et al. Cardiac myosin binding protein-C mutations in families with
620 hypertrophic cardiomyopathy: disease expression in relation to age, gender, and long
621 term outcome. *Circ Cardiovasc Genet* **5**, 156-166 (2012).
622 30. Kimura, A. et al. Mutations in the cardiac troponin I gene associated with hypertrophic
623 cardiomyopathy. *Nat Genet* **16**, 379-382 (1997).

624 31. Watkins, H. et al. Mutations in the genes for cardiac troponin T and alpha-tropomyosin
625 in hypertrophic cardiomyopathy. *N Engl J Med* **332**, 1058-1064 (1995).
626 32. Mogensen, J. et al. Alpha-cardiac actin is a novel disease gene in familial hypertrophic
627 cardiomyopathy. *J Clin Invest* **103**, R39-43 (1999).
628 33. Mavilakandy, A. & Ahamed, H. Mutation of the MYL3 gene in a patient with mid-
629 ventricular obstructive hypertrophic cardiomyopathy. *BMJ Case Rep* **15** (2022).
630 34. Flavigny, J. et al. Identification of two novel mutations in the ventricular regulatory
631 myosin light chain gene (MYL2) associated with familial and classical forms of
632 hypertrophic cardiomyopathy. *J Mol Med (Berl)* **76**, 208-214 (1998).
633 35. Alfieri, C.M., Evans-Anderson, H.J. & Yutzey, K.E. Developmental regulation of the
634 mouse IGF-I exon 1 promoter region by calcineurin activation of NFAT in skeletal
635 muscle. *Am J Physiol Cell Physiol* **292**, C1887-1894 (2007).
636 36. Knoll, R. Myosin binding protein C: implications for signal-transduction. *J Muscle Res*
637 *Cell Motil* **33**, 31-42 (2012).
638 37. Wang, M. et al. TRPA1 deficiency attenuates cardiac fibrosis via regulating
639 GRK5/NFAT signaling in diabetic rats. *Biochem Pharmacol* **214**, 115671 (2023).
640 38. Saygili, E. et al. The angiotensin-calcineurin-NFAT pathway mediates stretch-induced
641 up-regulation of matrix metalloproteinases-2/-9 in atrial myocytes. *Basic Res Cardiol*
642 **104**, 435-448 (2009).
643 39. Deschamps, A.M. & Spinale, F.G. Pathways of matrix metalloproteinase induction in
644 heart failure: bioactive molecules and transcriptional regulation. *Cardiovasc Res* **69**,
645 666-676 (2006).
646 40. Fan, D., Takawale, A., Lee, J. & Kassiri, Z. Cardiac fibroblasts, fibrosis and
647 extracellular matrix remodeling in heart disease. *Fibrogenesis Tissue Repair* **5**, 15
648 (2012).
649 41. Eghbali, M. Cardiac fibroblasts: function, regulation of gene expression, and phenotypic
650 modulation. *Basic Res Cardiol* **87 Suppl 2**, 183-189 (1992).
651 42. Butt, R.P., Laurent, G.J. & Bishop, J.E. Collagen production and replication by cardiac
652 fibroblasts is enhanced in response to diverse classes of growth factors. *Eur J Cell Biol*
653 **68**, 330-335 (1995).
654 43. Matsusaka, H. et al. Targeted deletion of matrix metalloproteinase 2 ameliorates
655 myocardial remodeling in mice with chronic pressure overload. *Hypertension* **47**, 711-
656 717 (2006).
657 44. Heymans, S. et al. Loss or inhibition of uPA or MMP-9 attenuates LV remodeling and
658 dysfunction after acute pressure overload in mice. *Am J Pathol* **166**, 15-25 (2005).

659 45. Lu, J. et al. Amlodipine and Atorvastatin Improved Hypertensive Cardiac Remodeling
660 through Regulation of MMPs/TIMPs in SHR Rats. *Cell Physiol Biochem* **39**, 47-60
661 (2016).
662 46. Varo, N. et al. Chronic AT(1) blockade stimulates extracellular collagen type I
663 degradation and reverses myocardial fibrosis in spontaneously hypertensive rats.
664 *Hypertension* **35**, 1197-1202 (2000).
665 47. Yang, L. et al. VEGF increases the proliferative capacity and eNOS/NO levels of
666 endothelial progenitor cells through the calcineurin/NFAT signalling pathway. *Cell Biol*
667 *Int* **36**, 21-27 (2012).
668 48. Manabe, T., Park, H. & Minami, T. Calcineurin-nuclear factor for activated T cells
669 (NFAT) signaling in pathophysiology of wound healing. *Inflamm Regen* **41**, 26 (2021).
670 49. Jabr, R.I. et al. Nuclear translocation of calcineurin Abeta but not calcineurin Aalpha by
671 platelet-derived growth factor in rat aortic smooth muscle. *Am J Physiol Cell Physiol*
672 **292**, C2213-2225 (2007).
673 50. Minami, T. et al. The calcineurin-NFAT-angiopoietin-2 signaling axis in lung
674 endothelium is critical for the establishment of lung metastases. *Cell Rep* **4**, 709-723
675 (2013).
676 51. Oka, T., Akazawa, H., Naito, A.T. & Komuro, I. Angiogenesis and cardiac
677 hypertrophy: maintenance of cardiac function and causative roles in heart failure. *Circ*
678 *Res* **114**, 565-571 (2014).
679 52. Kutryk, M.J. & Stewart, D.J. Angiogenesis of the heart. *Microsc Res Tech* **60**, 138-158
680 (2003).
681 53. Carmeliet, P. & Jain, R.K. Molecular mechanisms and clinical applications of
682 angiogenesis. *Nature* **473**, 298-307 (2011).
683 54. Varricchi, G. et al. Angiopoietins, Vascular Endothelial Growth Factors and Secretory
684 Phospholipase A(2) in Ischemic and Non-Ischemic Heart Failure. *J Clin Med* **9** (2020).
685 55. Rotter, D. et al. Calcineurin and its regulator, RCAN1, confer time-of-day changes in
686 susceptibility of the heart to ischemia/reperfusion. *J Mol Cell Cardiol* **74**, 103-111
687 (2014).
688 56. deAlmeida, A.C., van Oort, R.J. & Wehrens, X.H. Transverse aortic constriction in
689 mice. *J Vis Exp* (2010).
690 57. Zaw, A.M., Williams, C.M., Law, H.K. & Chow, B.K. Minimally Invasive Transverse
691 Aortic Constriction in Mice. *J Vis Exp* (2017).
692 58. Liu, B., Li, A., Gao, M., Qin, Y. & Gong, G. Modified Protocol for A Mouse Heart
693 Failure Model Using Minimally Invasive Transverse Aortic Constriction. *STAR Protoc*
694 **1**, 100186 (2020).

695 59. Shiraishi, M., Yamaguchi, A. & Suzuki, K. Nrg1/ErbB signaling-mediated regulation of
696 fibrosis after myocardial infarction. *FASEB J* **36**, e22150 (2022).
697 60. Shiraishi, M. et al. Alternatively activated macrophages determine repair of the
698 infarcted adult murine heart. *J Clin Invest* **126**, 2151-2166 (2016).
699 61. Shiraishi, M., Kimura, N. & Yamaguchi, A. Early cardiac contractility outcome of
700 reoperative coronary artery bypass grafting using right gastroepiploic artery. *J Card*
701 *Surg* **36**, 4103-4110 (2021).
702 62. Garg, M. et al. Cardiolipin-mediated PPARgamma S112 phosphorylation impairs IL-10
703 production and inflammation resolution during bacterial pneumonia. *Cell Rep* **34**,
704 108736 (2021).
705

Acknowledgements

This project was supported by SENSHIN Medical Research Foundation, a Grant-in-Aid for Scientific Research (C), TERUMO LIFE SCIENCE FOUNDATION, Suzuken Memorial Foundation, Kato Memorial Trust for Nambyo Research, a grant from Bristol Myers Squibb for non-clinical research. The author thanks Ms. Wendy Alexander-Adams for her assistance in reporting the findings in English.

Author contributions

M.S. conceptualized and designed the study; performed the experiments, acquired, analyzed, and interpreted the data; and drafted and critically revised the manuscript.

Data availability statement

The author declares that all supporting data are available within the article and its online supplementary file. For purposes of reproducibility, additional technical information and data that support the findings of this study are available from the corresponding author on reasonable request. Microarray data can be obtained from Gene Expression Omnibus GSE270186 https://www.ncbi.nlm.nih.gov/geo/query/acc.cgi?acc=GSE270186

724 **Competing interests**

725 The author declares no competing interests.

726

727 **Figure legends**

728 **Figure 1. Heart released from transverse aortic constriction attenuates cardiac**

729 **hypertrophy, fibrosis, and angiogenesis.**

730 (**a**) Schematic representation of the *in vivo* experiment. Transverse aortic constriction (TAC)

731 was performed, followed by 8 weeks of observation (TAC heart). Heart was released from TAC

732 4 weeks after TAC surgery, reducing afterload, and this was followed by 4 weeks of observation

733 (TAC-R). Normal heart (NH) was used for control.

734 (**b**) Echocardiography revealed increased left ventricular posterior wall thickness at diastole

735 (LVPWd) and decreased left ventricular end-diastolic volume (LVEDV) and left ventricular

736 end-systolic volume (LVESV) in TAC heart relative to values in NH. Echocardiography also

737 improvement in these changes in TAC-R heart. Other measures of interest were interventricular

738 septal thickness at diastole (IVSd), left ventricular diastolic dimension (LVDd), left ventricular

739 systolic dimension (LVDs), stroke volume (SV), and left ventricular ejection fraction (LVEF). n

740 = 4 animals per group. *$p < .05$ versus the other group(s) by one-way ANOVA.

741 (**c**) Cardiac troponin T staining showed a significant increase in the cross-sectional area around

742 the short-axis of individual cardiomyocytes (viewed from the transverse section) in TAC heart.

743 TAC release contributed to the decrease in this area in cardiomyocytes in TAC-R heart. scale

744 bars: 50 μm in low magnification. scale bars: 10 μm in high magnification. n = 4 animals per

745 group; mean ± SEM values are shown. *p < .05, **p < .01, ***p < .005, ****p < .001 versus

746 the other group(s) by one-way ANOVA.

747 (**d**) Masson's trichrome staining showed increased collagen deposition in TAC heart. TAC

748 release contributed to the decreased collagen deposition in TAC-R heart.

749 (**e**) Isolectin B4 staining showed increased capillary density in TAC heart. TAC release

750 contributed to the decreased capillary density in TAC-R heart.

751 (**d-e**), scale bars: 100 μm. n = 4 animals per group; mean ± SEM values are shown. *p < .05,

752 **p < .01, ***p < .005, ****p < .001 versus the other group(s) by one-way ANOVA.

753

754 **Figure 2. Gene expression analysis pertaining to cardiac hypertrophy, fibrosis, and**

755 **angiogenesis.**

756 (**a**) qRT-PCR showed hypertrophy-associated genes (*Igf1, Mybpc3, Tnni3, Tnnt2, Actc1, Myl2,*

757 and *Myl3*) to be upregulated, most (but not all) significantly upregulated in TAC heart relative

758 to expression in normal heart (NH). Expression of these genes was then shown to be decreased

759 in TAC-R heart relative to expression in NH.

760 (**b**) qRT-PCR showed fibrosis-associated genes (*Col1a1, Col3a1, Mmp2, Mmp9, Tgfb1, Acta2,*

761 *Timp1,* and *Fn1*) to be upregulated, some (but not all) significantly upregulated in TAC heart.

762 The trend was similar in TAC-R heart.

763 (**c**) qRT-PCR showed angiogenesis-associated genes (*Vegfa, Fgf1, Fgf2, Fgf9, Pdgfb,* and

764 *Angpt2*) to be upregulated, some (but not all) significantly upregulated, in TAC heart. These

765 genes were shown to be downregulated, some significantly downregulated, in TAC-R heart.

766 (**d**) qRT-PCR showed inflammation-associated genes (*IL1b* and *TNFa*) to be upregulated, some

767 significantly upregulated, in TAC heart. These genes were shown to be downregulated in heart

768 TAC-R heart.

769 (**a-d**), n = 4 animals per group; mean ± SEM values are shown. *p < .05, **p < .01, ***p

770 < .005, ****p < .001 versus the other group(s) by one-way ANOVA.

771

772 **Figure 3. Reperfusion following left ventricular loading increases oxidative stress.**

773 (**a**) Principal component analysis clearly revealed distinct grouping of normal heart (NH), TAC

774 heart, and TAC-R heart, indicating that TAC and TAC-R hearts have unique gene expression

775 patterns compared with NH.

776 (**b**) The top 20 significantly enriched molecules are displayed in the heatmap. The heatmap cells
777 are colored according to their p-values, with white indicating lack of enrichment for that term in
778 the corresponding gene list.
779 (**c**) Average mitochondrial DNA (mtDNA) copy number showed mitochondrial function to be
780 significantly attenuated in TAC heart. In TAC-R heart, average mtDNA copy number was
781 further decreased.
782 (**d**) Comprehensive gene expression analysis showed significant changes in the expression of 14
783 genes associated with Gene Ontology term "Response to oxidative stress" including *Rcan1*.
784 (**e**) qRT-PCR showed revealed *Rcan1* to be significantly upregulated in TAC-R heart. n = 4
785 animals per group; mean ± SEM values are shown. *$p < .05$ versus the other group(s) by one-
786 way ANOVA.
787 (**f**) Schematic representation and overview of the calcineurin-nuclear factor of activated T cells
788 (NFAT) signaling pathway. NFAT proteins are typically located in the cytoplasm in a
789 phosphorylated, inactive state. Various stressors can directly activate calcineurin, prompting the
790 dephosphorylation and subsequent nuclear translocation of NFAT. Once dephosphorylated by
791 calcineurin, NFAT proteins move from the cytoplasm to the nucleus, where they act as
792 transcription factors regulating genes involved in myocardial hypertrophy, fibrosis, and
793 angiogenesis.

794

795 **Figure 4. Knockdown of regulator of calcineurin 1 exacerbates hypertrophy and**

796 **attenuates cardiac contractility.**

797 (**a**) Schematic representation of the *in vivo* experiment. Regulator of calcineurin 1 (*Rcan1*)

798 siRNA or negative control (NC) siRNA combined with JetPEI® was injected into the tail vein of

799 rats 1 week after transverse aortic constriction (TAC) release (TAC-R heart), followed by a total

800 of three intravenous infusions (one given every other week).

801 (**b**) qRT-PCR showed *Rcan1* expression to be increased in heart released from TAC transfected

802 with NC siRNA. In contrast, its expression was markedly suppressed in TAC-R heart

803 transfected with *Rcan1* siRNA. n = 4 animals per group; mean ± SEM values are shown. *p

804 < .05, **p < .01, ***p < .005, ****p < .001 versus the other group(s) by one-way ANOVA.

805 (**c**) Representative M-mode echocardiography tracings of normal heart (NH) and TAC-R heart

806 transfected with NC *Rcan1* siRNA or *Rcan1* siRNA.

807 (**d**) Echocardiography revealed increased left ventricular wall thickness and decreased left

808 ventricular end diastolic and end systolic volumes (LVEDV and LVESV) in TAC heart at 4

809 weeks after TAC surgery, and improvement in such changes in TAC-R heart transfected with

810 NC siRNA at 8 weeks after surgery. *Rcan1* knockdown further increased left ventricular

811 posterior wall thickness and decreased left ventricular volume, and it attenuated LVEF in TAC-

812 R heart examined at 8 weeks after surgery. n = 4 animals per group. *p < .05 versus the other

813 group(s) by one-way ANOVA; $^{\#}P<0.05$ versus the same group at 4 weeks after surgery by

814 paired t-test.

815

816 TAC-R (NC), heart released from TAC transfected with NC siRNA; TAC-R (*Rcan1* KD), heart

817 released from TAC transfected with *Rcan1* siRNA; IVSd, interventricular septal thickness at

818 diastole; LVPWd, left ventricular posterior wall thickness at diastole; LVDd, left ventricular

819 diastolic dimension; LVDs, left ventricular systolic dimension; LVEDV, left ventricular end-

820 diastolic volume; LVESV, left ventricular end-systolic volume; SV, stroke volume; EF, ejection

821 fraction.

822

823 **Figure 5. Regulator of calcineurin 1 knockdown (KD) exacerbates hypertrophy, fibrosis**

824 **and angiogenesis in heart.**

825 (**a**) Body weight change (upper graph) and its ratio (lower graph) of normal heart (NH), Heart

826 released from TAC transfected with negative control (NC) siRNA (TAC-R [NC]) or *Rcan1*

827 siRNA (TAC-R [*Rcan1* KD]).

828 (**b**) Representative images of NH and TAC-R (NC) and TAC-R (*Rcan1* KD) hearts. Heart

829 weight (HW)/body weight (BW) ratio (mg/g) was markedly increased in TAC-R (*Rcan1* KD)

830 heart.

831 (**c**) Representative images of the cross-sectional area around the short-axis of individual

832 cardiomyocytes (viewed from the transverse section) of NH and TAC-R (NC), and TAC-R

833 (*Rcan1* KD) hearts. Interventricular septal thickness (IVST) was markedly increased in TAC-R

834 (*Rcan1* KD) heart.

835 (**d**) Cardiac troponin T staining showed significantly increased area of short-axis transverse

836 section of cardiomyocyte in TAC-R (*Rcan1* KD) heart.

837 (**e**) Masson's trichrome staining showed significantly increased collagen deposition in TAC-R

838 (*Rcan1* KD) heart.

839 (**f**) Isolectin B4 staining showed increased capillary density in TAC-R (*Rcan1* KD) heart.

840 (a) n = 4 animals per group. *p < .05 versus the other group(s) by one-way ANOVA; (b, c) scale

841 bars: 10 mm; (d) scale bars: 50 μm in low magnification. scale bars: 10 μm in high

842 magnification; (e, f) scale bars: 100 μm; (**a–e**) n = 4 animals per group; mean ± SEM values are

843 shown. *p < .05, **p < .01, ***p < .005, ****p < .001 versus the other group(s) by one-way

844 ANOVA.

845

846 **Figure 6. Knockdown of regulator of calcineurin 1 affects expression of genes related to**

847 **cardiac hypertrophy, fibrosis, and angiogenesis.**

848 (**a**) qRT-PCR revealed upregulated expression of hypertrophy-associated genes (*Igf1, Mybpc3,*

849 *Tnnt2, Tpm1, Actc1, Myl2* and *Myl3*) in TAC-R heart transfected with *Rcan1* siRNA (TAC-R

850 [*Rcan1* KD]) relative to expression in normal heart and TAC-R heart transfected with negative

851 control (NC) siRNA (TAC-R [NC]).

852 (**b**) qRT-PCR revealed significantly upregulated expression of fibrosis-associated genes

853 (*Col3a1, Tgfb1, Timp1,* and *Fn1*) in TAC-R (*Rcan1* KD) heart relative to that in normal heart

854 and/or TAC-R (NC) heart.

855 (**c**) qRT-PCR revealed significantly upregulated expression of angiogenesis-associated genes

856 (*Fgf1, Fgf2,* and *Fgf9*) in TAC-R (*Rcan1* KD) heart relative to that in normal heart and/or TAC-

857 R NC heart.

858 (**a–c**) n = 4 animals per group; mean ± SEM values are shown. *p < .05, **p < .01, ***p < .005,

859 ****p < .001 versus the other group(s) by one-way ANOVA.

860

861 **Figure 7. Schematic representation and overview of reversibility of hemodynamic changes**

862 **in the heart.**

863 Increased left ventricular afterload resulting from transverse aortic constriction (TAC) promotes

864 cardiac hypertrophy, fibrosis, and angiogenesis. In contrast, reduction in afterload by TAC

865 release (TAC-R) attenuates these changes. The structural change in the heart involves

866 modulation of the activity of the calcineurin nuclear factor of activated T cells (NFAT)

867 signaling pathway, with a potential regulator of calcineurin 1.

Name	p-value	Odds Ratio
Regulation of mitochondrion organization (GO: 0010821)	0.3672	2.23
Regulation of cytokine production involved in inflammatory response (GO:1900015)	0.3436	2.43
Inflammatory response (GO:0006954)	0.3636	1.41
Positive regulation of inflammatory response (GO:0050729)	0.6145	1.06
Regulation of inflammatory response (GO:0050727)	0.6446	0.91
Rho protein signal transduction (GO:0007266)	0.3787	2.14
Negative regulation of calcineurin-NFAT signaling cascade (GO:0070885)	0.0957	10.94
Regulation of calcineurin-NFAT signaling cascade (GO:0070884)*	0.2673	3.31

Table 1 Gene Ontology (GO) terms associated with maintenance of mitochondrial function, inhibition of inflammation, inhibition of Rho kinase activity, and inhibition of calcineurin-NFAT signaling.

*Negative regulation of calcineurin-NFAT signaling cascade (GO:0070885) is more involved in the effects of release from TAC than in other biological processes.

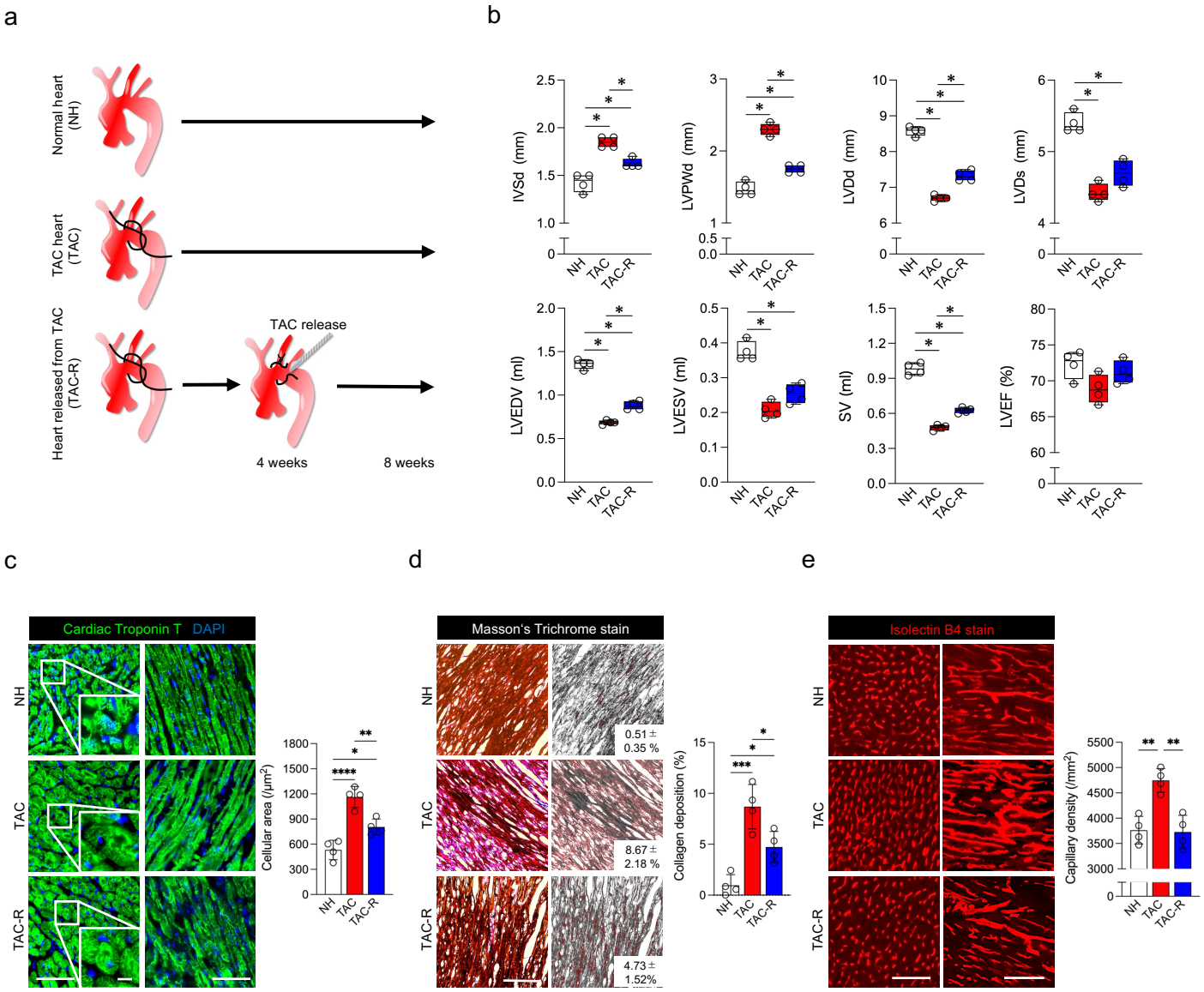
a
Normal heart (NH)
TAC heart (TAC)
Heart released from TAC (TAC-R)
TAC release
4 weeks
8 weeks
b
IVSd (mm)
LVPWd (mm)
LVDd (mm)
LVDs (mm)
LVEDV (ml)
LVESV (ml)
SV (ml)
LVEF (%)
NH
TAC
TAC-R
c
Cardiac Troponin T DAPI
Cellular area (/μm²)
d
Masson's Trichrome stain
0.51 ± 0.35 %
8.67 ± 2.18 %
4.73 ± 1.52%
Collagen deposition (%)
e
Isolectin B4 stain
Capillary density (/mm²)

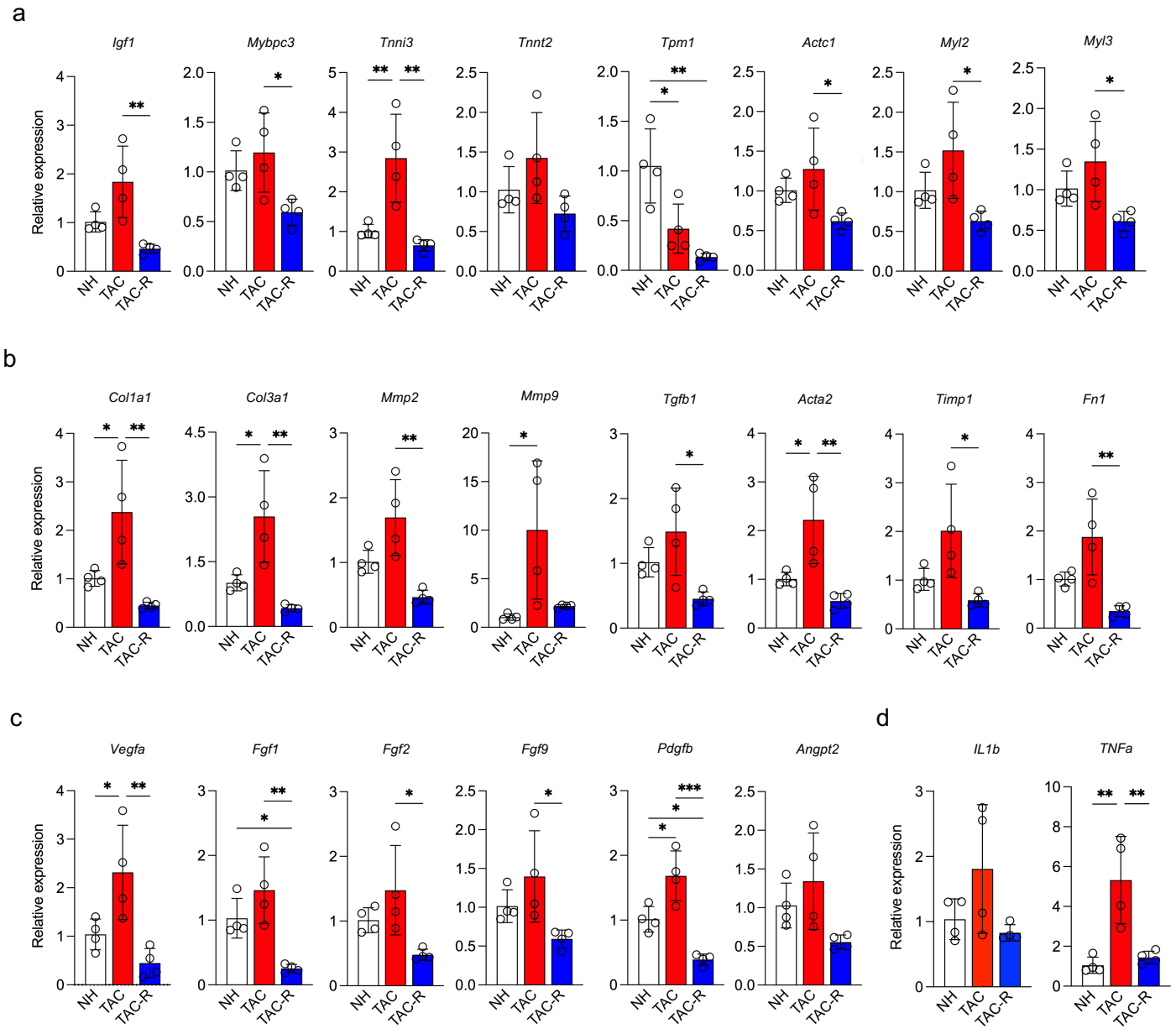
a
Igf1
Mybpc3
Tnni3
Tnnt2
Tpm1
Actc1
Myl2
Myl3
b
Col1a1
Col3a1
Mmp2
Mmp9
Tgfb1
Acta2
Timp1
Fn1
c
Vegfa
Fgf1
Fgf2
Fgf9
Pdgfb
Angpt2
d
IL1b
TNFa
Relative expression
NH
TAC
TAC-R

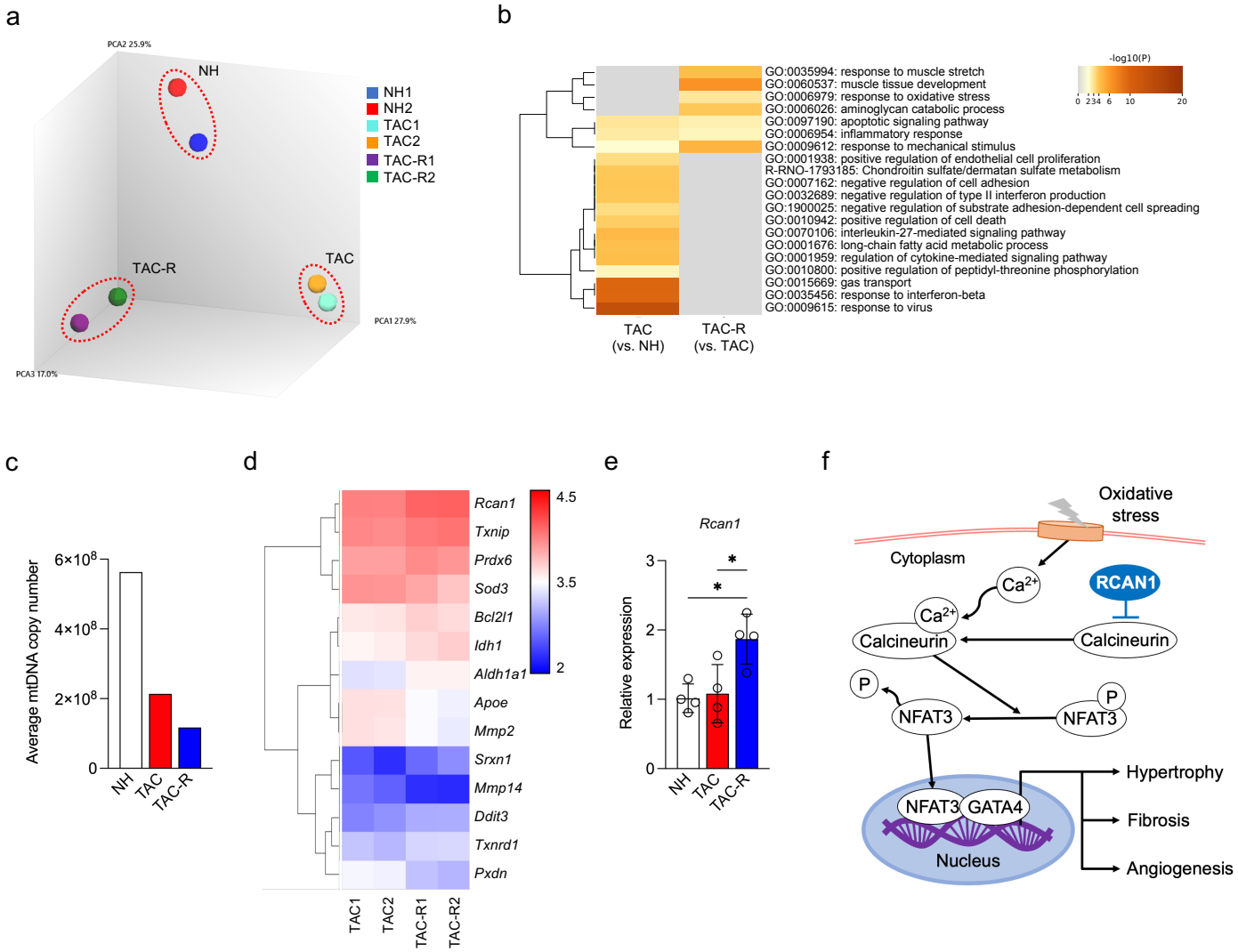
a
PCA2 25.9%
NH
TAC-R
TAC
PCA1 27.9%
PCA3 17.0%
NH1
NH2
TAC1
TAC2
TAC-R1
TAC-R2
b
-log10(P)
0 2 3 4 6 10 20
GO:0035994: response to muscle stretch
GO:0060537: muscle tissue development
GO:0006979: response to oxidative stress
GO:0006026: aminoglycan catabolic process
GO:0097190: apoptotic signaling pathway
GO:0006954: inflammatory response
GO:0009612: response to mechanical stimulus
GO:0001938: positive regulation of endothelial cell proliferation
R-RNO-1793185: Chondroitin sulfate/dermatan sulfate metabolism
GO:0007162: negative regulation of cell adhesion
GO:0032689: negative regulation of type II interferon production
GO:1900025: negative regulation of substrate adhesion-dependent cell spreading
GO:0010942: positive regulation of cell death
GO:0070106: interleukin-27-mediated signaling pathway
GO:0001676: long-chain fatty acid metabolic process
GO:0001959: regulation of cytokine-mediated signaling pathway
GO:0010800: positive regulation of peptidyl-threonine phosphorylation
GO:0015669: gas transport
GO:0035456: response to interferon-beta
GO:0009615: response to virus
TAC (vs. NH)
TAC-R (vs. TAC)
c
Average mtDNA copy number
6×10^8
4×10^8
2×10^8
0
NH
TAC
TAC-R
d
Rcan1
Txnip
Prdx6
Sod3
Bcl2l1
Idh1
Aldh1a1
Apoe
Mmp2
Srxn1
Mmp14
Ddit3
Txnrd1
Pxdn
4.5
3.5
2
TAC1
TAC2
TAC-R1
TAC-R2
e
Rcan1
Relative expression
3
2
1
0
*
*
NH
TAC
TAC-R
f
Oxidative stress
Cytoplasm
Ca2+
Ca2+
RCAN1
Calcineurin
Calcineurin
P
NFAT3
P
NFAT3
NFAT3
GATA4
Nucleus
Hypertrophy
Fibrosis
Angiogenesis

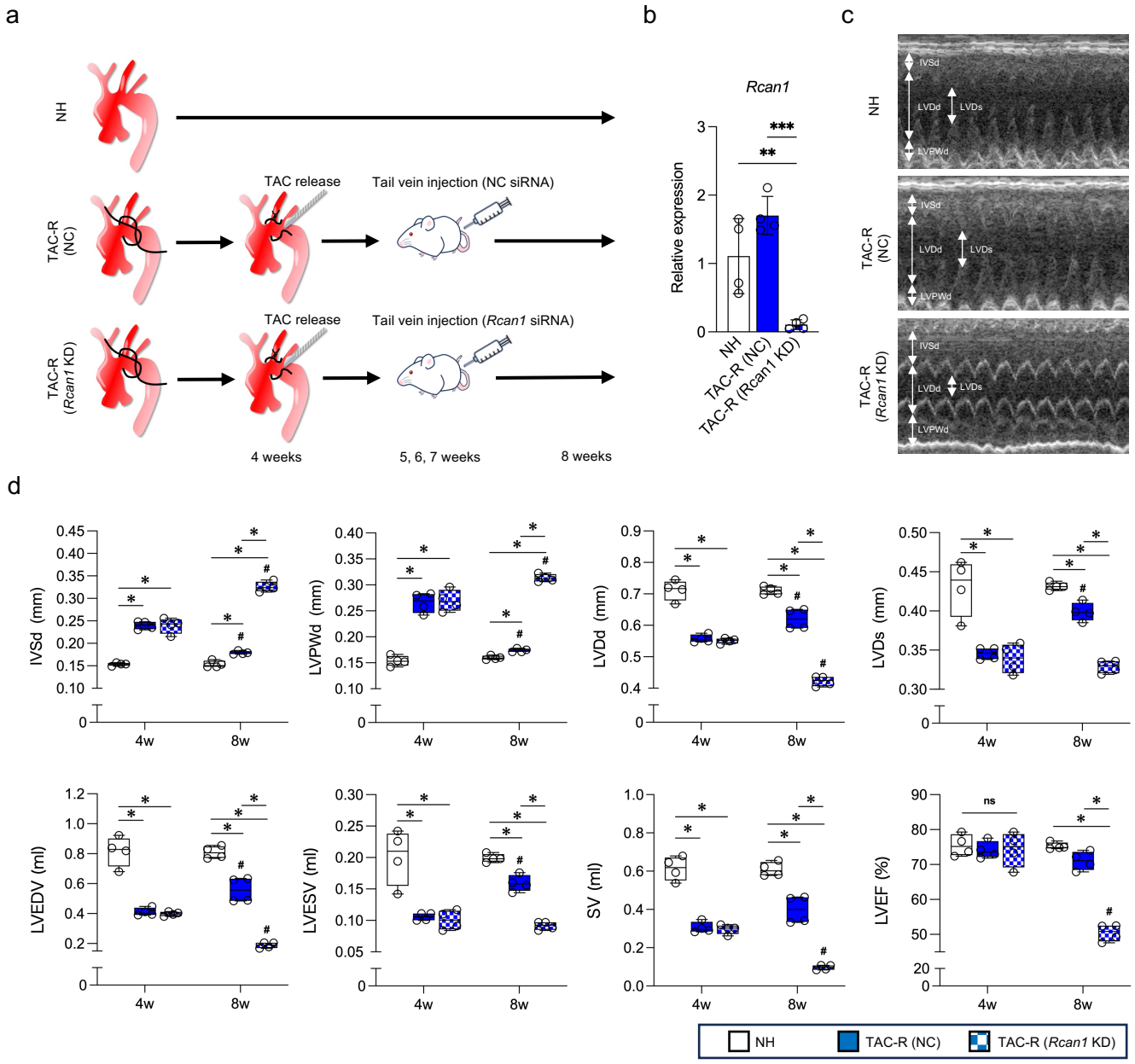
a
NH
TAC-R (NC)
TAC-R (Rcan1 KD)
TAC release
Tail vein injection (NC siRNA)
Tail vein injection (Rcan1 siRNA)
4 weeks
5, 6, 7 weeks
8 weeks
b
Rcan1
Relative expression
NH
TAC-R (NC)
TAC-R (Rcan1 KD)
c
IVSd
LVDd
LVDs
LVPWd
d
IVSd (mm)
LVPWd (mm)
LVDd (mm)
LVDs (mm)
LVEDV (ml)
LVESV (ml)
SV (ml)
LVEF (%)
4w
8w
ns
NH
TAC-R (NC)
TAC-R (Rcan1 KD)

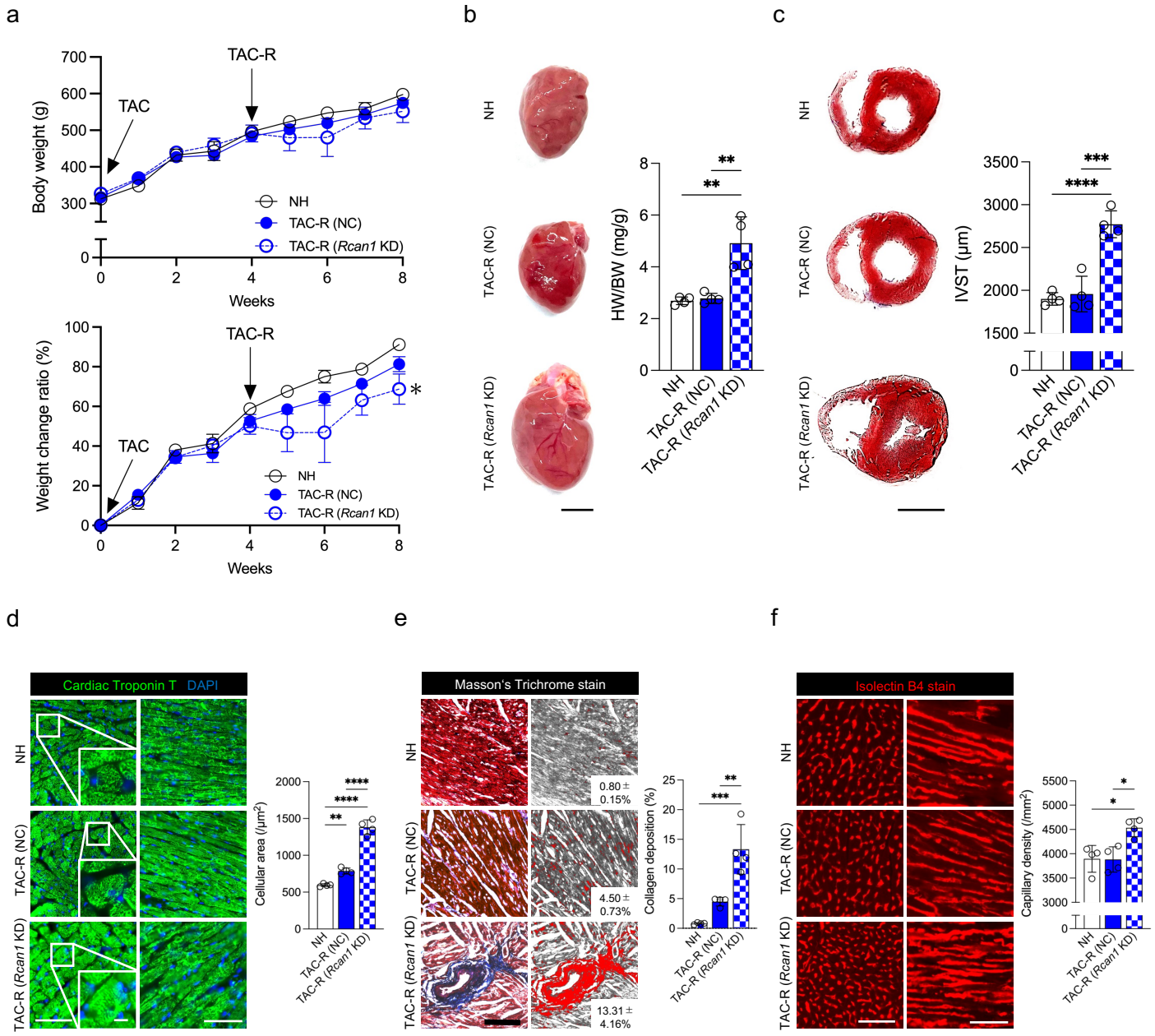
a
Body weight (g)
TAC
TAC-R
NH
TAC-R (NC)
TAC-R (Rcan1 KD)
Weeks
Weight change ratio (%)
b
HW/BW (mg/g)
c
IVST (μm)
d
Cardiac Troponin T DAPI
Cellular area (/μm²)
e
Masson's Trichrome stain
0.80 ± 0.15%
4.50 ± 0.73%
13.31 ± 4.16%
Collagen deposition (%)
f
Isolectin B4 stain
Capillary density (/mm²)

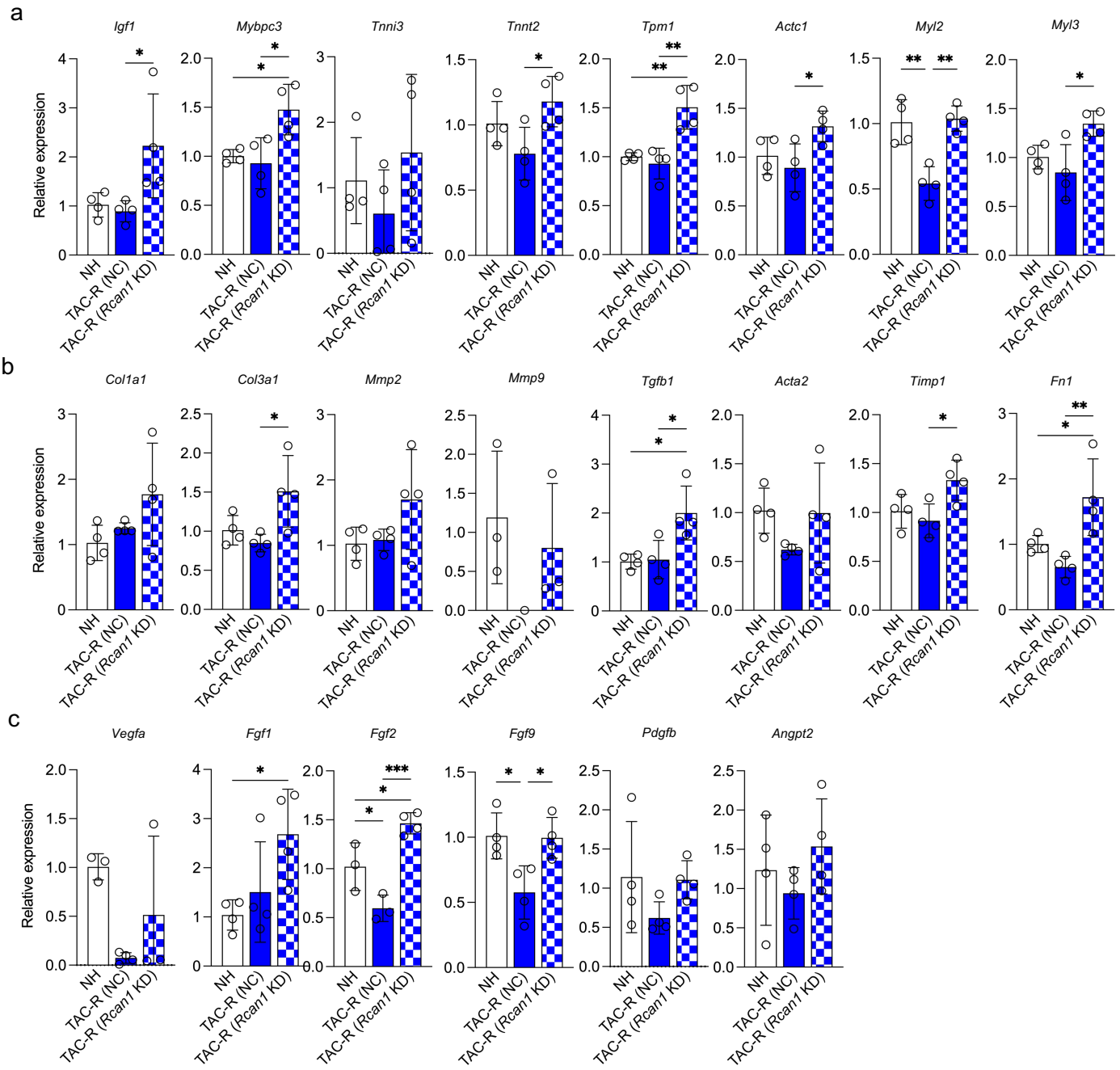
a
Igf1
Mybpc3
Tnni3
Tnnt2
Tpm1
Actc1
Myl2
Myl3
b
Col1a1
Col3a1
Mmp2
Mmp9
Tgfb1
Acta2
Timp1
Fn1
c
Vegfa
Fgf1
Fgf2
Fgf9
Pdgfb
Angpt2
Relative expression
NH
TAC-R (NC)
TAC-R (Rcan1 KD)

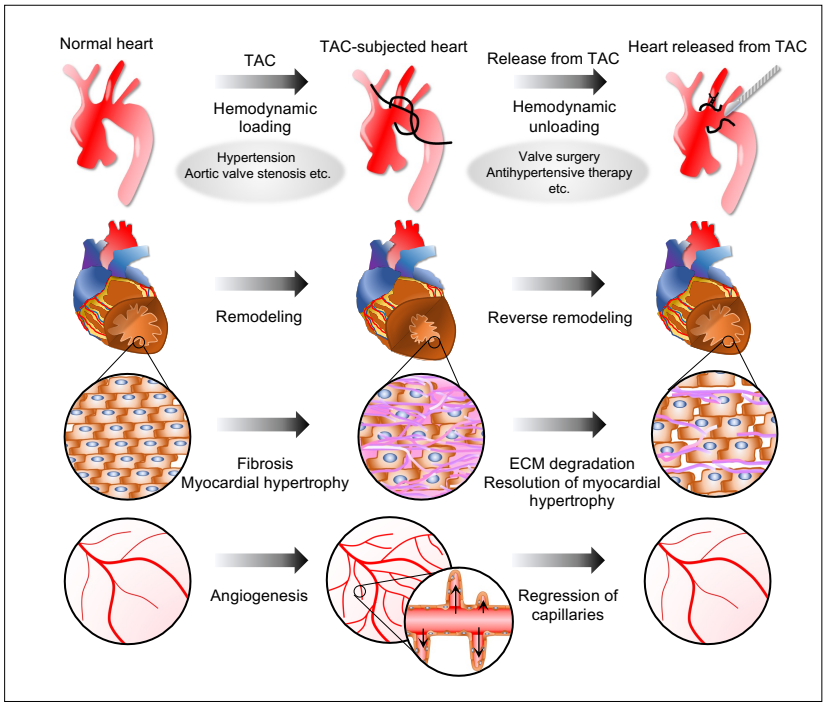
Normal heart
TAC
Hemodynamic loading
Hypertension
Aortic valve stenosis etc.
TAC-subjected heart
Release from TAC
Hemodynamic unloading
Valve surgery
Antihypertensive therapy
etc.
Heart released from TAC
Remodeling
Reverse remodeling
Fibrosis
Myocardial hypertrophy
ECM degradation
Resolution of myocardial hypertrophy
Angiogenesis
Regression of capillaries

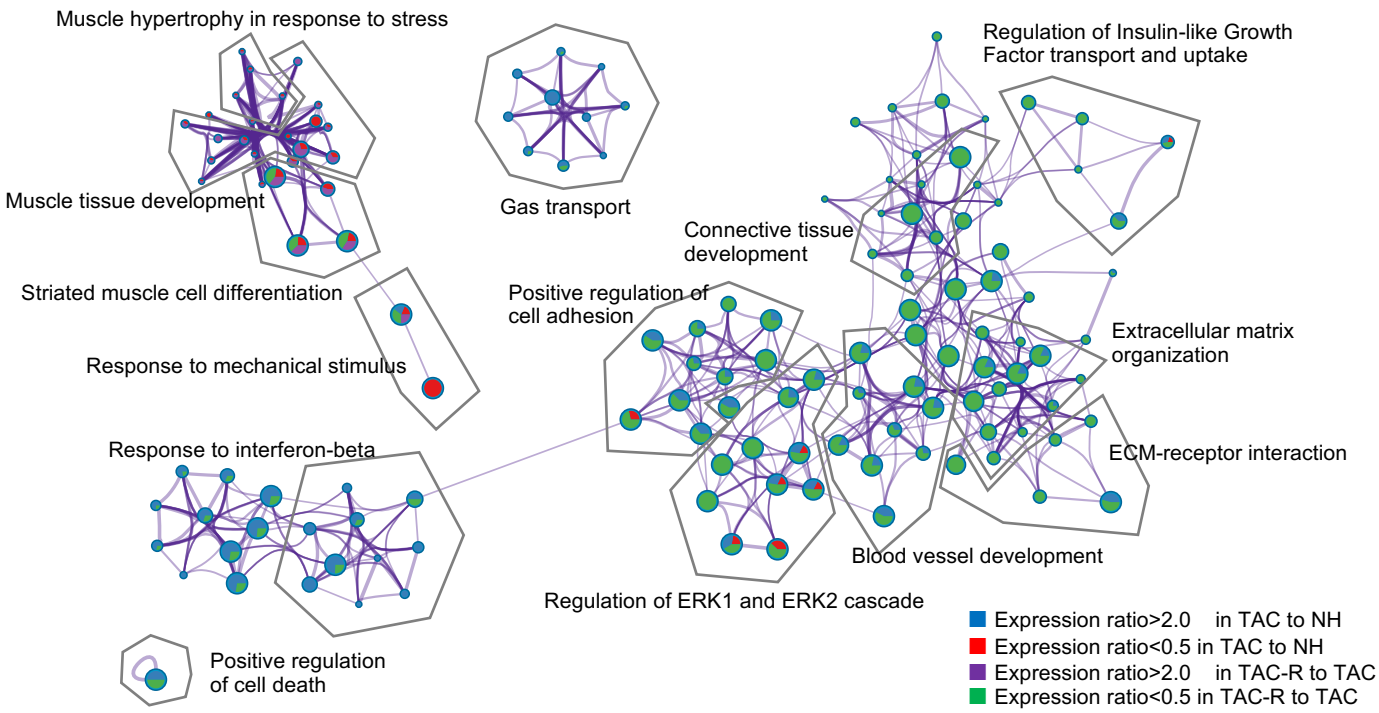

Supplementary Figure 1. Subset of representative terms and network layout.
Each term is represented by a circular node, with the size of each node proportional to the number of input genes that fall under that term and the color of each node indicative of its cluster identity. Terms with a similarity score > 0.3 are linked. Thickness of the edge represents the similarity score. The Cytoscape layout is force-directed. Each term label serves as an aggregate of the labels in each cluster.